Supporting Information for

Spontaneous Resolution of Racemic Cage-Catenanes via Diastereomeric Enrichment at Molecular Level and Subsequent Narcissistic Self-Sorting at Supramolecular Level

Pan Li[†], Zhongwei Sun[†], Jiaolong Chen[†], Yong Zuo[†], Chunyang Yu[†], Xiaoning Liu[†], Zhenyu Yang[†], Lihua Chen[†], Enguang Fu[†], Weihao Wang[†], Jiacheng Zhang[†], Zhiqiang Liu[‡*], Jinming Hu[§*], and Shaodong Zhang[†*]

[†]School of Chemistry and Chemical Engineering, Shanghai Jiao Tong University, 800 Dongchuan Road, Shanghai 200240, China.

[‡]The National and Local Joint Engineering Research Center for Biomanufacturing of Chiral Chemicals, Zhejiang University of Technology, Hangzhou 310014, P. R. China.

[§]CAS Key Laboratory of Soft Matter Chemistry, Department of Polymer Science and Engineering, University of Science and Technology of China, Hefei 230026, Anhui, China.

Table of Contents

1. Genaral Information

1. 1 Materials

General reagents were purchased from commercial suppliers and used without further purification, unless otherwise indicated. Tetrakis(triphenylphosphine)palladium was purchased from Beijing J&K Chemical Co. Ltd. Butane-1,3-diol, triformylbenzene, 3,5-dibromobenzaldehyde, 3-nitrobenzeneboronic acid, boron trifluoride etherate, stannous chloride dihydrate and sodium triacetoxyborohydride were purchased from Shanghai Adamas-Beta Co. Ltd. 3,5-Di(3-nitrophenyl)benzaldehyde was synthesized according to our published procedures.[S1] Tetrahydrofuran and hexanes were dried over sodium and freshly distilled under nitrogen before use.

1. 2 Instruments

Nuclear Magnetic Resonance (NMR) spectra were recorded on a Bruker Advance III HD 400 spectrometer at room temperature. Chemical shift values (δ) are reported in ppm relative to the proton residual of the deutrated solvents, and coupling constants (J) are reported in Hertz (Hz).

Matrix-assisted laser desorption and ionization time-of-flight mass spectrometry (MALDI-TOF-MS) was performed on a solariX XR 7.0 T hybrid quadrupole-FTICR mass spectrometer, using DCTB (10 mg/mL in $CHCl_3$) as the matrix. The mass spectra were analyzed using Compass Data Analysis 5.0 (Bruker).

Analytical HPLC was conducted on a Shimadzu LC-20AD system using CHIRALPAK columns (0.46 cm I.D. × 25 cm L). Chromatographic condition for *rac*-**2**: AD-H column, methanol/acetonitrile/isopropanol = 90 : 10 : 0.1, 0.5 mL/min, UV detection at 254 nm, at 30 °C. Chromatographic condition for homochiral cage-catenanes (***R***, ***S***)^6-**3**, (***S***, ***R***)^6-**3**, (***R***, ***R***)^6-**3**, (***S***, ***S***)^6-**3**, and racemic cage-catenanes *rac*-**3**, *rac*-**3'** and *rac*-**3"**: IA column, chloroform/toluene/methanol/diethylamin = 20 : 20 : 60 : 0.1, 0.6 mL/min, UV detection at 295 nm, at 30 °C. Chromatographic condition for (***R***, ***S***)^6-**4** and (***S***, ***R***)^6-**4**: IF column, tetrahydrofuran/hexanes /methanol/diethylamin = 15 : 70 : 15 : 0.1, 0.6 mL/min, UV detection at 254 nm, at 35 °C.

Preparative HPLC was conducted on a YMC K-PreLAB 100S system at 35 °C with ~75% yield. Chromatographic conditions for *rac*-**2**: CHIRALPAK column AD (2.5 cm I.D. × 25 cm L), ethanol/acetonitrile = 90 : 10, 25 mL/min, UV detection at 214 nm.

Circular dichroism (CD) as performed with a Jasco J-1500 spectrometer. Solution spectra of chiral presursors were recorded in 1 mm quartz cuvettes using chloroform as solvent at 25 °C. A scan rate of 200 nm min^{-1} with a response time of 1 s and a bandwidth of 1 nm were adopted. Solution spectra of chiral cage-catenanes were recorded in 10 mm quartz cuvettes using tetrahydrofuran as solvent at 25 °C. A scan rate of 100 nm min^{-1} with a response time of 1 s and a bandwidth of 1 nm were adopted.

The optical rotations of all chiral compounds were measured in chloroform at 23 °C using a Jasco P-2000 polarimeter at a wavelength of 589 nm. For chiral compounds and homochiral cage-catenanes, solutions at 0.01 g/mL were prepared.

Single crystal X-ray diffraction (SC-XRD) data was collected on a Bruker D8 Venture diffractometer. The crystal was kept at 170.0 K during data collection. Using Olex2,[S2] the structures were solved with the SHELXT[S3] structure solution program using Intrinsic Phasing and refined with the SHELXL[S4] refinement package using Least Squares minimisation.

1. 3 Theoretical calculations

Geometry optimization and total energy calculations of the isomeric linkers (***S***, ***R***)-**2**, (***R***, ***S***)-**2**, (***R***, ***R***)-**2** and (***S***, ***S***)-**2** were performed with the Gaussian09 program[S5] at B3LYP/6-31G* without any symmetry restriction.[S6-S8] After the geometry optimization was performed, analytical vibration frequencies were calculated at the same level to determine the nature of the located stationary point.

2. Synthesis of Precursors and Cage-Catenanes

The syntheses of all chemical compounds are described as follows. ^{1}H and ^{13}C NMR resonances of all compounds are listed after their synthetic procedures and their assignments are given in NMR spectra in **Section 8**, unless otherwise indicated.

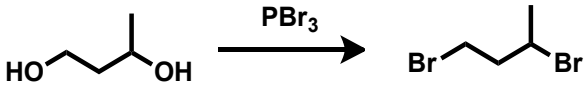

1,3-Dibromobutane: Under a nitrogen atmosphere, butane-1,3-diol (5.00 g, 55.0 mmol) and liquid PBr_3 (15.0 g, 5 mL, 110 mmol) were sequentially added in an ice bath to get a viscous liquid. The mixture was heated to 60 ºC for 2 h under strring, and the evolved hydrogen bromide was discharged into $NaHCO_3$ aqueous solution. Upon cooling to room temperature, iced water was added to quench the reaction and hexanes were used for extraction. The collected organic phase was neutralized with $NaHCO_3$ aqueous solution, dried over anhydrous Na_2SO_4, and concentrated to yield a clear liquid (7.5 g, 63% yield). ^{1}H NMR (400 MHz, $CDCl_3$) δ 4.31–4.23 (m, 1H), 3.54–3.50 (m, 2H), 2.32–2.15 (m, 2H), 1.73 (d, J = 6.8 Hz, 3H). ^{13}C NMR (101 MHz, $CDCl_3$) δ 48.60, 43.22, 31.34, 26.19. GC-MS: Calcd for $C_4H_8Br_2$ $[M+H]^+$ 215.897; Found, 215.900.

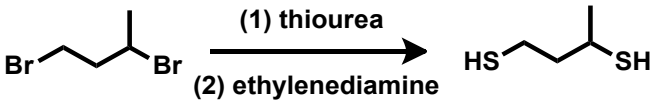

Butane-1,3-dithiol: Thiourea (1.92 g, 25.3 mmol) and 1,3-dibromobutane (2.60 g, 12.0 mmol) were refluxed in water (20 mL) under a nitrogen atmosphere for 4 h to yield a homogeneous solution. After cooling to 0 ºC in an ice bath, ethylenediamine (1.66 g, 1.84 ml, 27.7 mmol) was added dropwise under vigorous stirring, Then, the mixture was heated to reflux again for 12 h. The reaction mixture was extracted by ether, dried over anhydrous Na_2SO_4, and concentrated to yield a yellow liquid (617 mg, 42% yield) which was used directly in the next step without further purification.

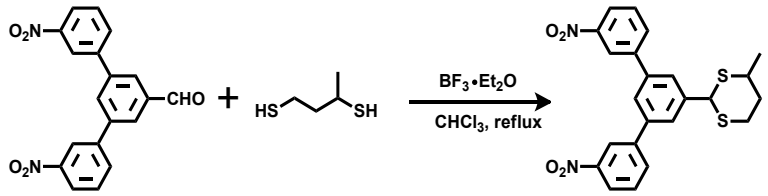

***rac*-2-(3,5-Di(3-nitrophenyl)phenyl)-4-methyl-1,3-dithiane** (*rac*-**DNPMD**): Under a nitrogen atmosphere, 3,5-di(3-nitrophenyl)benzaldehyde (5.10 g, 14.6 mmol) was suspended in 150 mL of chloroform, followed by the sequential addition of butane-1,3-dithiol (2.68 g, 22.0 mmol) and $BF_3 \cdot OEt_2$ (3.12 g, 22.0 mmol). The mixture was heated to reflux for 12 h, and quenched by 2 M NaOH aqueous solution. The collected organic phase was dried over anhydrous Na_2SO_4, concentrated and purified by column chromatography (petroleum ether/dichloromethane = 3 : 2, v/v) to yield a white solid (4.20 g, 62% yield) as the pure product. ^{1}H NMR (400 MHz, $CDCl_3$) δ 8.50 (s, 2H), 8.27 (d, J = 8.0 Hz, 2H), 7.99 (d, J = 8.0 Hz, 2H), 7.78 (s, 2H), 7.66 (t, J = 8.0 Hz, 2H), 5.45 (s, 0.1H), 5.33 (s, 0.9H), 3.14–3.07 (m, 3H), 2.25 (m, 1H), 1.72–1.66 (m, 1H), 1.32 (d, J = 6.8 Hz, 3H). MALDI-TOF MS Calcd for $C_{23}H_{20}N_2O_4S_2$ $[M+H]^+$ 453.090; Found, 453.108.

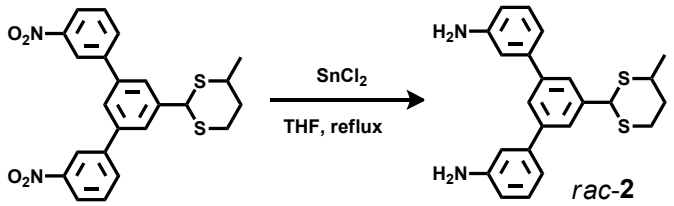

2-(3,5-Di(3-aminophenyl)phenyl)-4-methyl-1,3-dithiane (*rac*-**2**): To a solution of compound *rac*-**DNPMD** (2.0 g, 4.4 mmol) in THF (200 mL) was added stannous chloride dihydrate (9.9 g, 44.2 mmol). The mixture was stirred and heated to reflux for 12 h and then cooled to room temperature. The yellow solution was quenched with saturated $NaHCO_3$ solution and the organic phase was collected. After extracting the aqueous phase with EtOAc (3 × 100 mL), the combined organic phases were concentrated. The crude product was further purified by column chromatography (ethyl acetate/petroleum ether = 1 : 1, v/v) to yield the product as a white solid (1.42 g, 82% yield). ^{1}H NMR (400 MHz, $CDCl_3$) δ 7.75 (s, 0.2 H), 7.69 (s, 1H), 7.62 (s, 1.8 H), 7.26 (t, J = 8 Hz, 2H), 7.03 (d, J = 8 Hz, 2H), 6.95 (s, 2H), 6.69 (d, J = 8 Hz, 2H), 5.37 (s,

0.1H), 5.27 (s, 0.9H), 3.20–3.04 (m, 3H), 2.22 (m, 1H), 1.67 (m, 1H), 1.29–1.24 (m, 3H). MALDI-TOF MS Calcd for $C_{23}H_{24}N_2S_2$ $[M+H]^+$ 393.141; Found, 393.144.

Note: The peak at 5.37 ppm, assignable to the methine proton of (***R***, ***R***)-**2**, (***S***, ***S***)-**2**, was clearly separated from that of (***S***, ***R***)-**2**, (***R***, ***S***)-**2** at 5.27 ppm. More convincing evidence can be obtained from the NMR spectra of enantiopure (***S***, ***R***)-**2**, (***R***, ***S***)-**2**, (***R***, ***R***)-**2** and (***S***, ***S***)-**2**, which are provided in **Section 7.** Their structural characterizations are listed as follows.

(***S***, ***R***)-**2** and (***R***, ***S***)-**2**: ^{1}H NMR (400 MHz, $CDCl_3$) δ 7.69 (t, J = 1.6 Hz, 1H), 7.62 (d, J = 1.6 Hz, 1H), 7.23 (t, J = 8.0 Hz, 2H), 7.04 (m, 2H), 6.95 (t, J = 1.6 Hz, 2H), 6.70–6.67 (m, 2H), 5.27 (s, 1H), 3.10–3.04 (m, 3H), 2.84 (br, 4H), 2.22–2.18 (m, 1H), 1.70–1.61 (m, 1H), 1.29 (d, J = 6.8 Hz, 3H). ^{13}C NMR (101 MHz, $CDCl_3$) δ 146.84, 142.43, 142.04, 139.58, 129.81, 126.20, 125.60, 117.93, 114.45, 114.14, 52.88, 41.07, 34.14, 32.79, 21.85.

(***R***, ***R***)-**2** and (***S***, ***S***)-**2**: ^{1}H NMR (400 MHz, $CDCl_3$) δ 7.75 (d, J = 1.2 Hz, 2H), 7.67 (t, J = 1.6 Hz, 1H), 7.24 (t, J = 8.0 Hz, 2H), 7.05 (d, J = 8.0 Hz, 2H), 6.96 (t, J = 2.0 Hz, 2H), 6.71–6.68 (dd, J = 8.0 Hz, 1.6 Hz, 2H), 5.37 (s, 1H), 3.74 (br, 2H), 3.22–3.16 (m, 2H), 2.81–2.75 (m, 1H), 2.26–2.20 (m, 1H), 1.97–1.90 (m, 1H), 1.52 (d, J = 7.2 Hz, 3H). ^{13}C NMR (101 MHz, $CDCl_3$) δ 146.87, 142.25, 142.14, 140.10, 129.81, 126.08, 125.84, 117.89, 114.43, 114.12, 45.23, 35.69, 31.91, 26.11, 20.48.

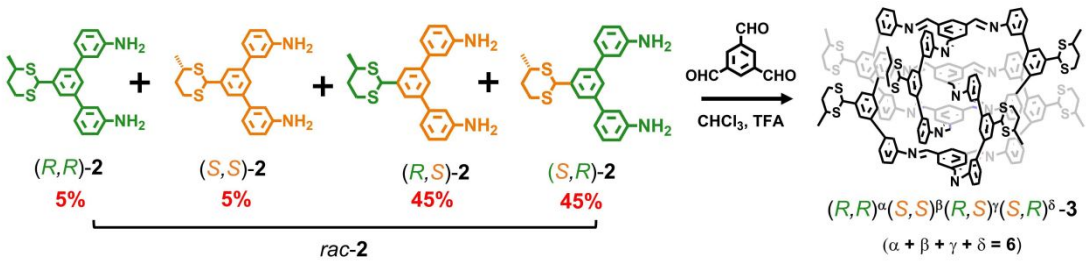

(***R***,***R***)$^{\alpha}$(***S***,***S***)$^{\beta}$(***S***,***R***)$^{\gamma}$(***R***,***S***)$^{\delta}$-**3** (*rac*-**3**): Diamine linker *rac*-**2** (200 mg, 0.51 mmol, 1.5 equiv.) was dissolved in chloroform (100 mL), followed by adding catalytic amount of TFA (0.1 mmol, 0.1 equiv.) to afford a slightly turbid solution. A solution of 1,3,5-triformylbenzene (100 mg, 0.34 mmol, 1.0 equiv.) was then added dropwise. The imine condensation reaction proceeded for 48 h to maximize the cage-catenane yield.

Purification of the target *rac*-**3** was performed on flash chromatographic column packed with silica gel with tertiary solvents of THF/hexanes/triethylamine (1: 1 : 0.05), affording a light yellow solid (154 mg, 65% yield). ^{1}H NMR (400 MHz, $CDCl_3$) δ 8.40 (s, 6H), 8.23 (s, 6H), 7.93 (s, 6H), 7.79 (s, 6H), 7.74 (s, 6H), 7.67 (s, 6H), 7.64 (s, 6H), 7.5 (d, J = 8 Hz, 6H), 7.43 (t, J = 8 Hz, 6H), 7.4 (s, 6H), 7.16–7.10 (dd, J = 14.4 Hz, 8 Hz, 12H), 6.95 (s, 6H), 6.85 (t, J = 8 Hz, 6H), 6.80 (s, 6H), 5.33 (s, 0.6H), 5.22 (s, 5.4H), 3.07–3.00 (m, 18H), 2.20 (m, 6H), 1.69–1.60 (m, 6H), 1.28 (d, J = 6.8 Hz, 18H). MALDI-TOF MS Calcd for $C_{174}H_{144}N_{12}S_{12}$ $[M+H]^+$ 2787.840; Found, 2787.685.

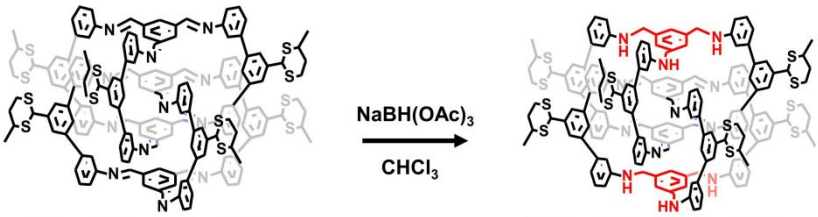

(*R*,*R*)$^\alpha$(*S*,*S*)$^\beta$(*R*,*S*)$^\gamma$(*S*,*R*)$^\delta$ **-3**

(α + β + γ + δ = **6**)

(*R*,*R*)$^\alpha$(*S*,*S*)$^\beta$(*R*,*S*)$^\gamma$(*S*,*R*)$^\delta$ **-4**

(α + β + γ + δ = **6**)

(***R***,***R***)$^\alpha$(***S***,***S***)$^\beta$(***S***,***R***)$^\gamma$(***R***,***S***)$^\delta$**-4** (*rac*-**4**): Imine-based *rac*-**3** (50 mg, 0.0179 mmol) was dissolved in chloroform (20 mL), and $NaBH(OAc)_3$ (1.68 g, 1.07 mmol) was added directly. The suspension was stirred at room temperature for 12 h, and then the solids were removed by filtration. The organic phase was neutralized with saturated $NaHCO_3$ solution, and then dried over $MgSO_4$. After concentrating to approximately 1/5 of its original volume, hexanes were added to precipitate the product as white solids (46 mg, 92% yield). ^{1}H NMR (400 MHz, $CDCl_3$) δ 8.40 (s, 6H), 8.02 (s, 6H), 7.76 (s, 6H), 7.64 (s, 12H), 7.37 (s, 6H), 7.29 (t, J = 8 Hz, 6H), 7.18 (d, J = 8 Hz, 6H), 7.11 (m, 12H), 6.97 (s, 6H), 6.93–6.89 (m, 12H), 6.66 (d, J = 8 Hz, 6H), 5.24 (s, 0.6H) 5.16 (s, 5.4H), 4.15 (s, 12H), 3.03–2.93 (m, 18H), 2.15 (d, J = 12.8 Hz, 6H), 1.62 (m, 6H), 1.22 (d, J = 7.2 Hz, 18H). MALDI-TOF MS Calcd for $C_{174}H_{156}N_{12}S_{12}$ $[M]^+$ 2798.926; Found, 2798.896.

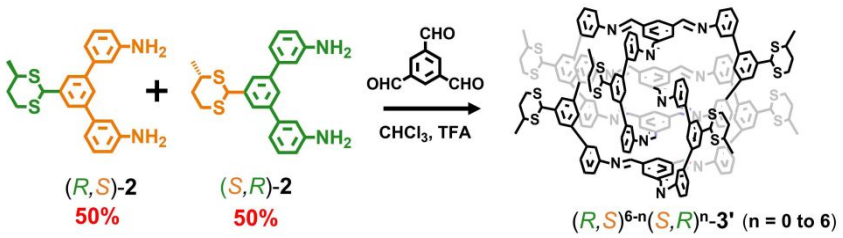

(***R***,***S***)$^{6-n}$(***S***,***R***)^{n}-**3'** (*rac*-**3'**): (***S***, ***R***)-**2** and (***R***, ***S***)-**2** in equal molar ratio (40 mg, 0.1 mmol, 1.5 equiv.) were dissolved in chloroform (20 mL), followed by adding catalytic amount of TFA (0.002 mmol, 0.1 equiv.) to afford a slightly turbid solution. A solution of 1,3,5-triformylbenzene (10.8 mg, 0.067 mmol, 1.0 equiv.) was then added dropwise. The imine condensation reaction proceeded for 48 h to maximize the cage-catenane yield. Purification of the target *rac*-**3'** followed same procedures as *rac*-**3** to yield a white solid (31 mg, 67% yield). ^{1}H NMR (400 MHz, $CDCl_3$) δ 8.40 (s, 6H), 8.23 (s, 6H), 7.93 (s, 6H), 7.79 (s, 6H), 7.74 (s, 6H), 7.67 (s, 6H), 7.64 (s, 6H), 7.5 (d, J = 8 Hz, 6H), 7.43 (t, J = 8 Hz, 6H), 7.4 (s, 6H), 7.16–7.10 (dd, J = 14.4 Hz, 8 Hz, 12H), 6.95 (s, 6H), 6.85 (t, J = 8 Hz, 6H), 6.80 (s, 6H), 5.22 (s, 6H), 3.07–3.00 (m, 18H), 2.21–2.17 (m, 6H), 1.69–1.60 (m, 6H), 1.28 (d, J = 6.8 Hz, 18H).

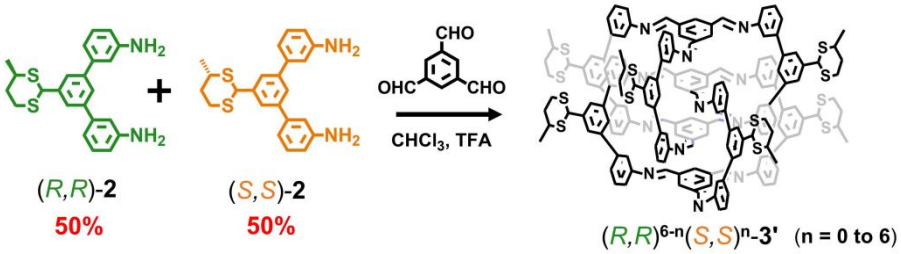

(***R***,***R***)$^{6-n}$(***S***,***S***)^{n}-**3''** (*rac*-**3''**): Following the same synthetic procedures as *rac*-**3'**, *rac*-**3''** prepared from (***S***, ***R***)-**2** and (***R***, ***S***)-**2** in equal molar ratio were purified to yield a white solid (25 mg, 54% yield). ^{1}H NMR (400 MHz, $CDCl_3$) δ 8.40 (s, 6H), 8.23 (s, 6H), 7.92 (s, 6H), 7.79 (s, 6H), 7.76 (d, J = 6.8 Hz, 12H), 7.69 (s, 6H), 7.52–7.50 (m, 12H), 7.43 (t, J = 8 Hz, 6H), 7.16–7.10 (dd, J = 14.4 Hz, 8 Hz, 12H), 6.97 (s, 6H), 6.85 (t, J = 8 Hz, 6H), 6.80 (d, J = 8 Hz, 6H), 5.34 (s, 6H), 3.22–3.16 (m, 12H), 2.77–2.72 (m, 6H), 2.26–2.18 (m, 6H), 1.97–1.89 (m, 6H), 1.52 (d, J = 6.8 Hz, 18H).

Note: As for *rac*-**3**, *rac*-**4**, *rac*-**3'** and *rac*-**3''**, their ^{13}C NMR spectra were not collected due to the presence of various diastereomers in these mixtures.

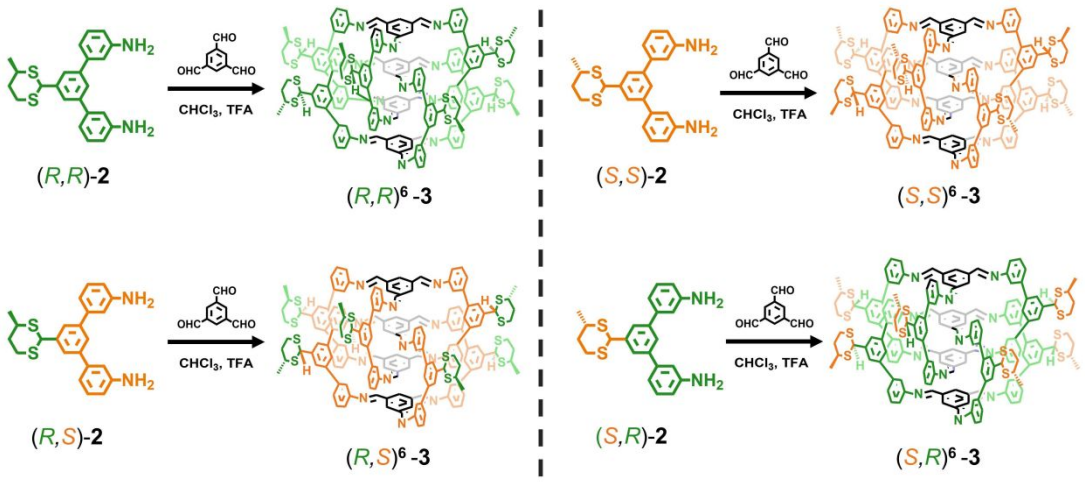

Enantiopure Cage-catenanes: Following the same synthetic procedures as *rac*-**3'**, four enantiopure cage-catenanes, namely (***R***, ***R***)^6-**3** and (***S***, ***S***)^6-**3**, (***R***, ***S***)^6-**3** and (***S***, ***R***)^6-**3**, were synthesized separately from the corresponding precursors, with yields ranging from 55% to 65%. The ^{1}H NMR, ^{13}C NMR and 2D COSY spectra are provided in **Section 7**. Their structural characterizations are listed as follows.

(***R***, ***R***)^6-**3** and (***S***, ***S***)^6-**3**: ^{1}H NMR (400 MHz, $CDCl_3$) δ 8.40 (s, 6H), 8.23 (s, 6H), 7.92 (s, 6H), 7.79 (s, 6H), 7.76 (d, J = 6.8 Hz, 6H), 7.69 (s, 6H), 7.52–7.50 (m, 12H), 7.43 (t, J = 8 Hz, 6H), 7.16–7.10 (dd, J = 14.4 Hz, 8 Hz, 12H), 6.97 (s, 6H), 6.85 (t, J = 8 Hz, 6H), 6.80 (d, J = 8 Hz, 6H), 5.34 (s, 6H), 3.22–3.16 (m, 12H), 2.77–2.72 (m, 6H), 2.26–2.18 (m, 6H), 1.97–1.89 (m, 6H), 1.52 (d, J = 6.8 Hz, 18H). ^{13}C NMR (101 MHz, $CDCl_3$) δ 160.20, 159.55, 153.90, 152.10, 142.02, 141.48, 140.88, 140.36, 139.54, 137.05, 136.96, 131.07, 130.09, 129.36, 128.74, 125.95, 125.38, 125.34, 124.34, 124.06, 123.99, 121.15, 118.48, 118.17, 52.88, 41.05, 34.17, 32.79, 21.87.

(***R***, ***S***)^6-**3** and (***S***, ***R***)^6-**3**: ^{1}H NMR (400 MHz, $CDCl_3$) δ 8.40 (s, 6H), 8.23 (s, 6H), 7.92 (s, 6H), 7.79 (s, 6H), 7.76 (d, J = 6.8 Hz, 6H), 7.69 (s, 6H), 7.52–7.50 (m, 12H), 7.43 (t, J = 8 Hz, 6H), 7.16–7.10 (dd, J = 14.4 Hz, 8 Hz, 12H), 6.97 (s, 6H), 6.85 (t, J = 8 Hz, 6H), 6.80 (d, J = 8 Hz, 6H), 5.34 (s, 6H), 3.22–3.16 (m, 12H), 2.77–2.72 (m, 6H), 2.26–2.18 (m, 6H), 1.97–1.89 (m, 6H), 1.52 (d, J = 6.8 Hz, 18H). ^{13}C NMR (101 MHz, $CDCl_3$) δ 160.16, 159.59, 153.94, 152.19, 142.09, 141.33, 140.72, 140.50, 140.09, 137.04, 136.97, 131.07, 130.11, 129.41, 128.74, 125.81, 125.78, 125.55, 124.32, 123.94, 121.17, 121.11, 118.44, 118.17, 45.16, 35.78, 29.86, 26.07, 24.43.

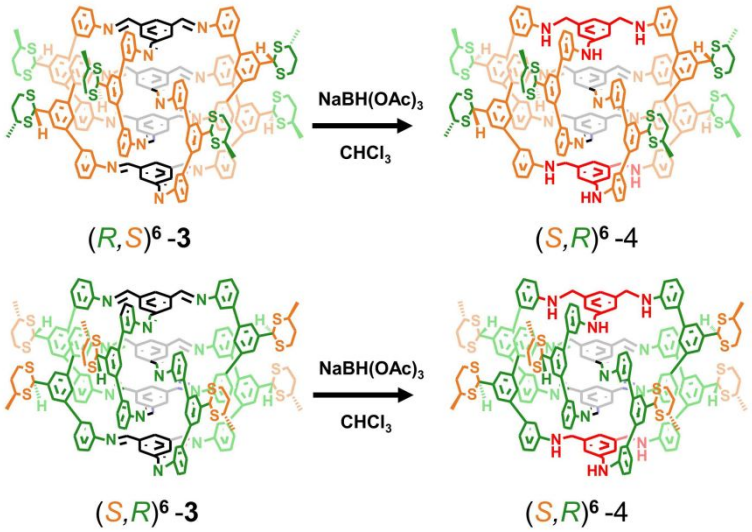

(***R***, ***S***)^6-**4** and (***S***, ***R***)^6-**4**: Pure (***R***, ***S***)^6-**3** or (***S***, ***R***)^6-**3** (30 mg, 0.0107 mmol) was dissolved in chloroform (20 mL), followed by adding NaBH $(OAc)_3$ (136 mg, 0.642 equiv.) to afford a suspension. The reaction was stirred at 25 ºC for 12 h, and the solids were removed by filtration. Then, aqueous $NaHCO_3$ was added for neutralization. The organic phase was collected, dried by Na_2SO_4 and concentrated to yield a white solid (29 mg, 97% yield).

(***R***, ***S***)^6-**4** and (***S***, ***R***)^6-**4**: ^{1}H NMR (400 MHz, $CDCl_3$) δ 8.40 (s, 6H), 8.02 (s, 6H), 7.76 (s, 6H), 7.64 (s, 6H), 7.37 (d, J = 6.8 Hz, 6H), 7.28 (t, J = 8 Hz, 6H), 7.18 (d, J = 7.2 Hz, 6H), 7.11–7.09 (m, 12H), 6.97 (s, 6 H), 6.91 (t, J = 8 Hz, 6H), 6.89 (s, 6H), 6.66 (d, J = 8 Hz, 6H), 5.16 (s, 6H), 4.15 (s, 12H), 3.90 (br, 6H), 3.03–2.92 (m, 18H), 2.16–2.13 (m, 6H), 1.65–1.56 (m, 6H), 1.24 (d, J = 6.8 Hz, 18H). ^{13}C NMR (101 MHz, $CDCl_3$) δ 159.80, 152.05, 148.94, 141.93, 141.24, 141.08, 141.02, 139.50, 138.87, 137.14, 129.98, 129.76, 129.08, 128.68, 125.95, 125.23, 125.17, 124.58, 121.66, 117.91, 116.73, 113.48, 111.87, 52.92, 41.01, 34.14, 32.76, 21.81.

3 CD Measurements

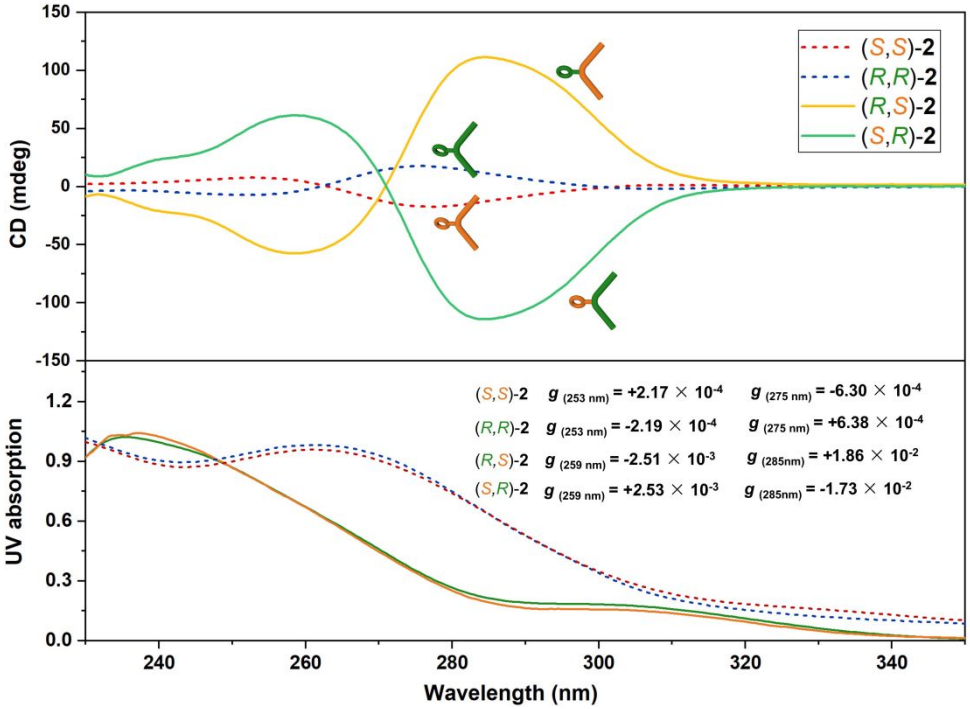

Figure S1. CD and UV/vis spectra of four enantiopure precursors in $CHCl_3$ solution (~3×10^{-4} M). Typical mirror-image bisignated signals were detected for the two pairs of enantiomers, showing two different zero-crossings at 270 nm for (***S***, ***R***)-**2** and (***R***, ***S***)-**2** (solid line), and at 262 nm for (***R***, ***R***)-**2** ad (***S***, ***S***)-**2** (dotted line), respectively.

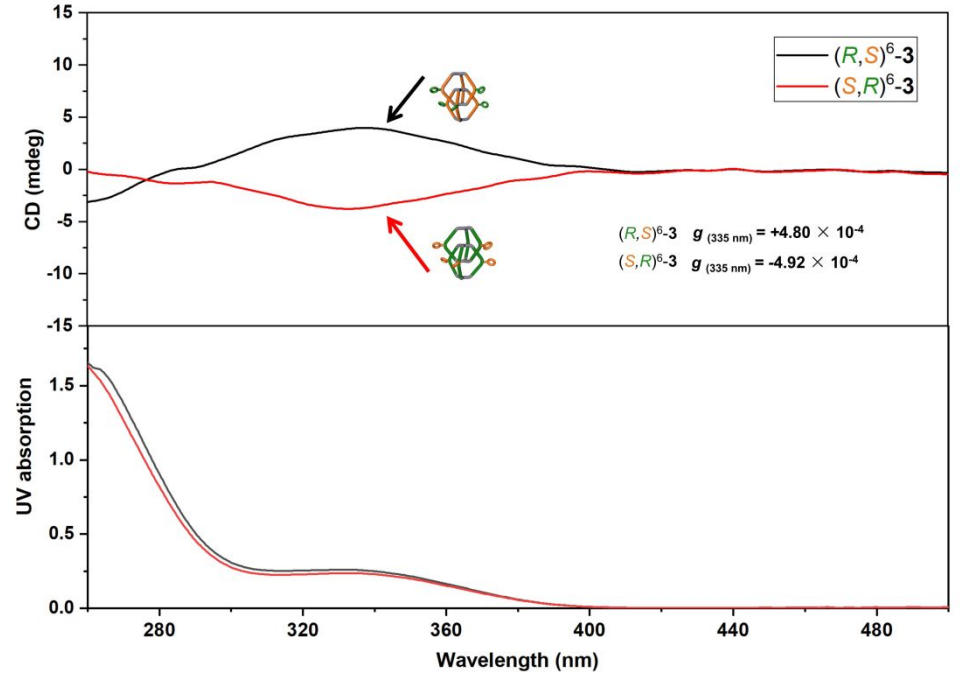

Figure S2. CD and UV/vis spectra of enantiopure cage-catenanes in THF solution (~5×10^{-5} M). Discernable CD signals were detected for both (***S***, ***R***)^6-**3** and (***R***, ***S***)^6-**3**.

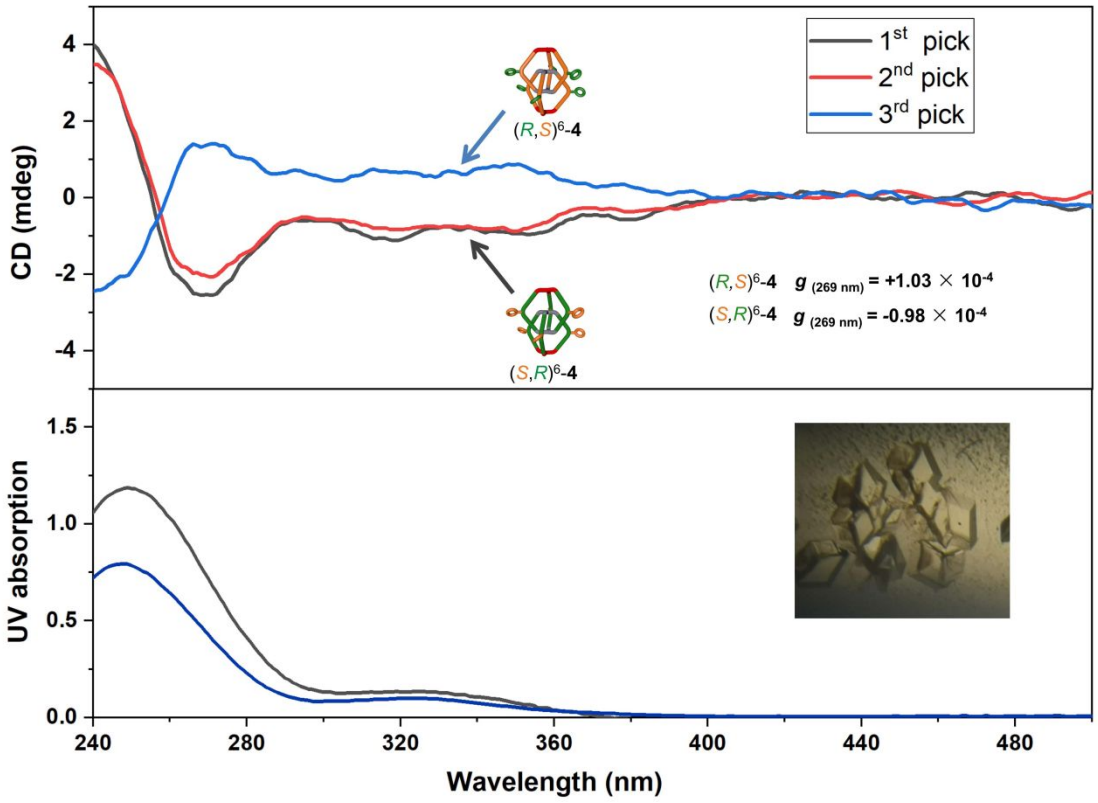

Figure S3. CD and UV/vis spectra of selected crystals formed in the solution of *rac*-**4** (i.e., (***R***,***R***)$^{\alpha}$(***S***,***S***)$^{\beta}$(***S***,***R***)$^{\gamma}$(***R***,***S***)$^{\delta}$-**4**). Discrete crystal was selected at random (three times) and washed gently with THF/ACN (v/v = 5:2) before re-dissolving in THF for measurement. Representative UV absorption spectra were used to calculate the dissymmetry factor "***g***". Inserted optical image is the typical morphology of picked crystals.

4 Optical Rotation Measurements

Table S1. The specific optical rotation values of all chiral compounds at 23 °C.

Sample	$[\alpha]_D$ (°)
(*S*, *R*)-**2**	+ 10.8
(*R*, *S*)-**2**	- 10.6
(*S*, *S*)-**2**	+ 8.3
(*R*, *R*)-**2**	- 8.7
(*S*, *R*)^6-**3**	+ 15.9
(*R*, S)^6-**3**	- 15.4
(*S*, *S*)^6-**3**	+ 13.5
(*R*, *R*)^6-**3**	- 13.7
(*S*, *R*)^6-**4**	+ 21.2
(*R*, S)^6-**4**	- 21.1

5. Diastereomers Calculations

The theoretical diastereomers after triply catenation can be analyzed by dissecting the cage-catenane into two individual monomeric cages. The upper and lower monomeric cage were denoted as **MC^{U} and MC^{L}**, respectively. Then, the catenation between **MC^{U} and MC^{L}** can be classified into three subgroups to conduct the calculation. To be specific, three subgroups are categorized as follows:

Group A: both **MC^{U}** and **MC^{L}** consist of homochiral linkers; **Group B**: either one of **MC^{U}** and **MC^{L}** consists of homochiral linkers, the other one consists of heterochiral linkers; **Group C**: both **MC^{U}** and **MC^{L}** consist of heterochiral linkers.

For easy analyses, four diastereomeric linkers are coded as 𝒶, 𝒷, 𝒸 and 𝒹, respectively. Then, for a specific **MC**, its three linkers can be described as a triplet of these four codes, including 𝒶𝒶𝒶, 𝒷𝒷𝒷, 𝒶𝒶𝒷, 𝒶𝒷𝒷, 𝒶𝒷𝒸, etc.

First, we consider the relatively simple situation when only two enantiomeric linkers take part in the formation of cage-catenanes. After excluding the duplicates, there are 3 + 4 + 9 = 16 types of theoretical diastereomers.

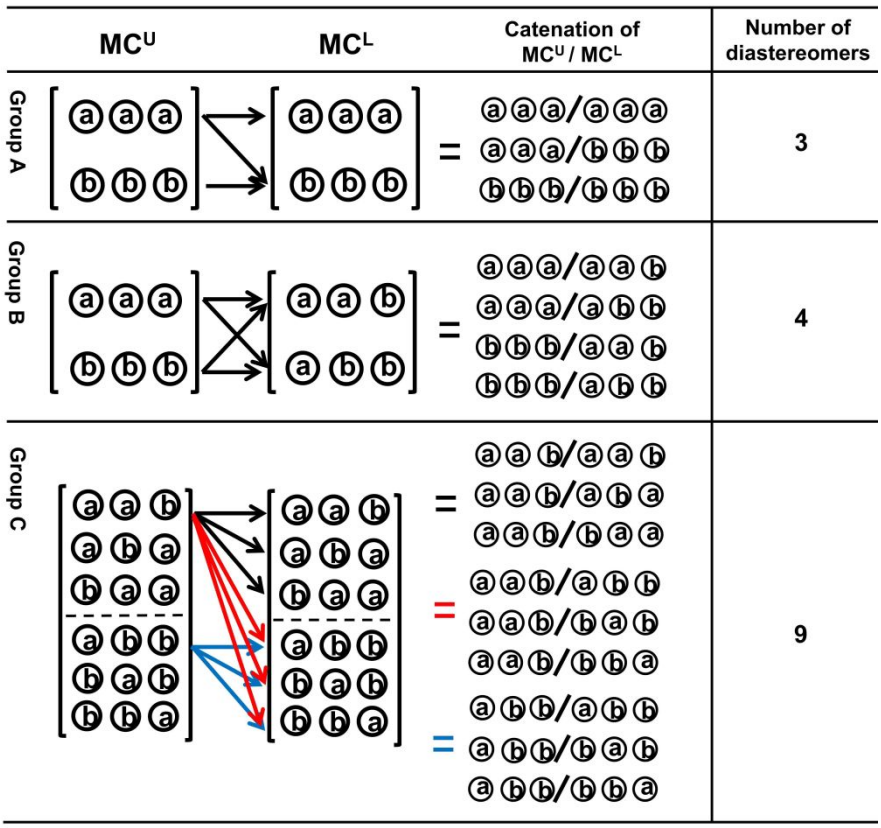

Then, we consider the situation when four diastereomeric linkers take part in the formation of cage-catenanes. After excluding the duplicates, there are 10 + 80 + 234 + 108 + 288 = 720 types of theoretical diastereomers. Detailed categories and calculated results were listed in the table below.

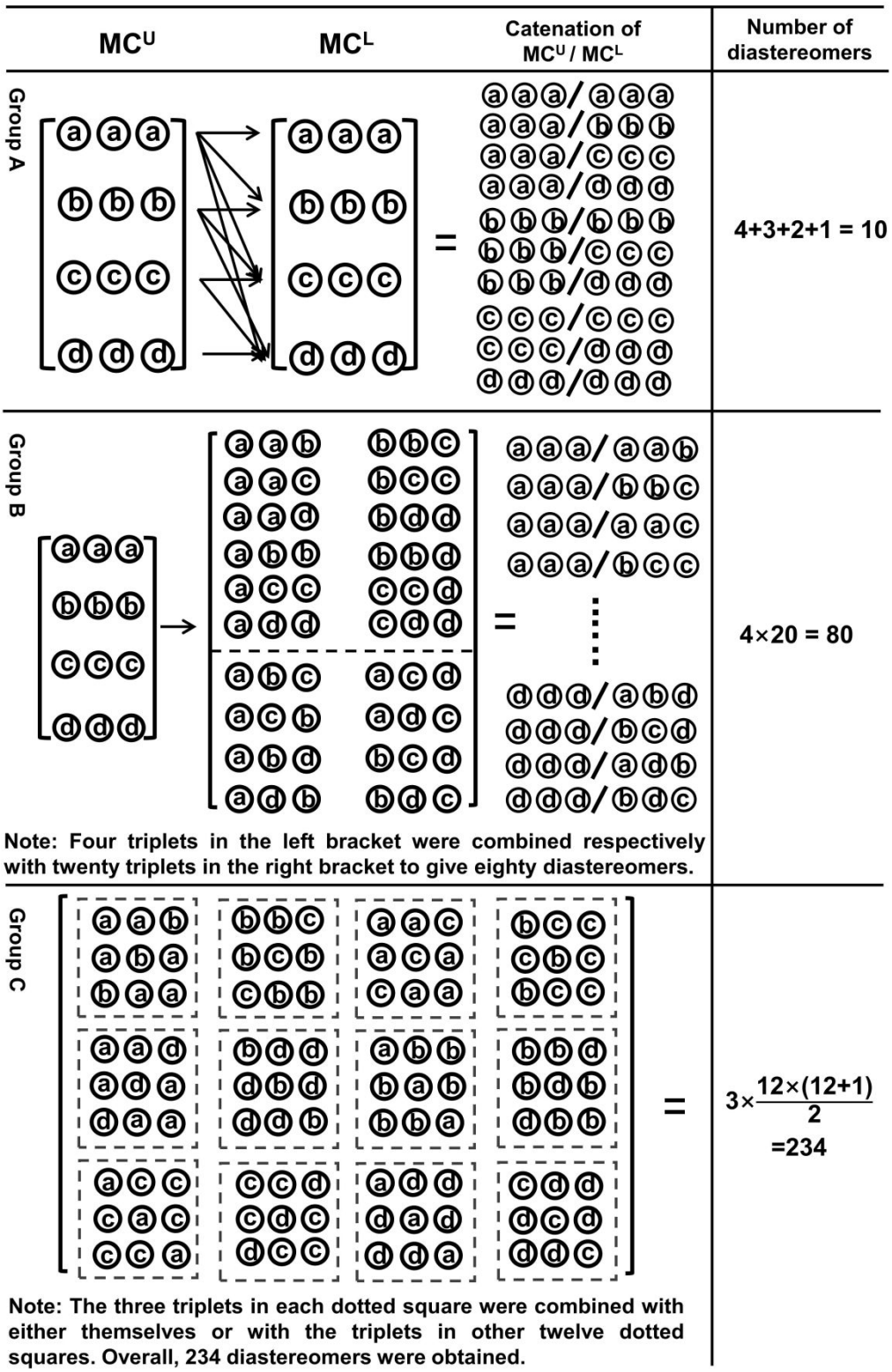

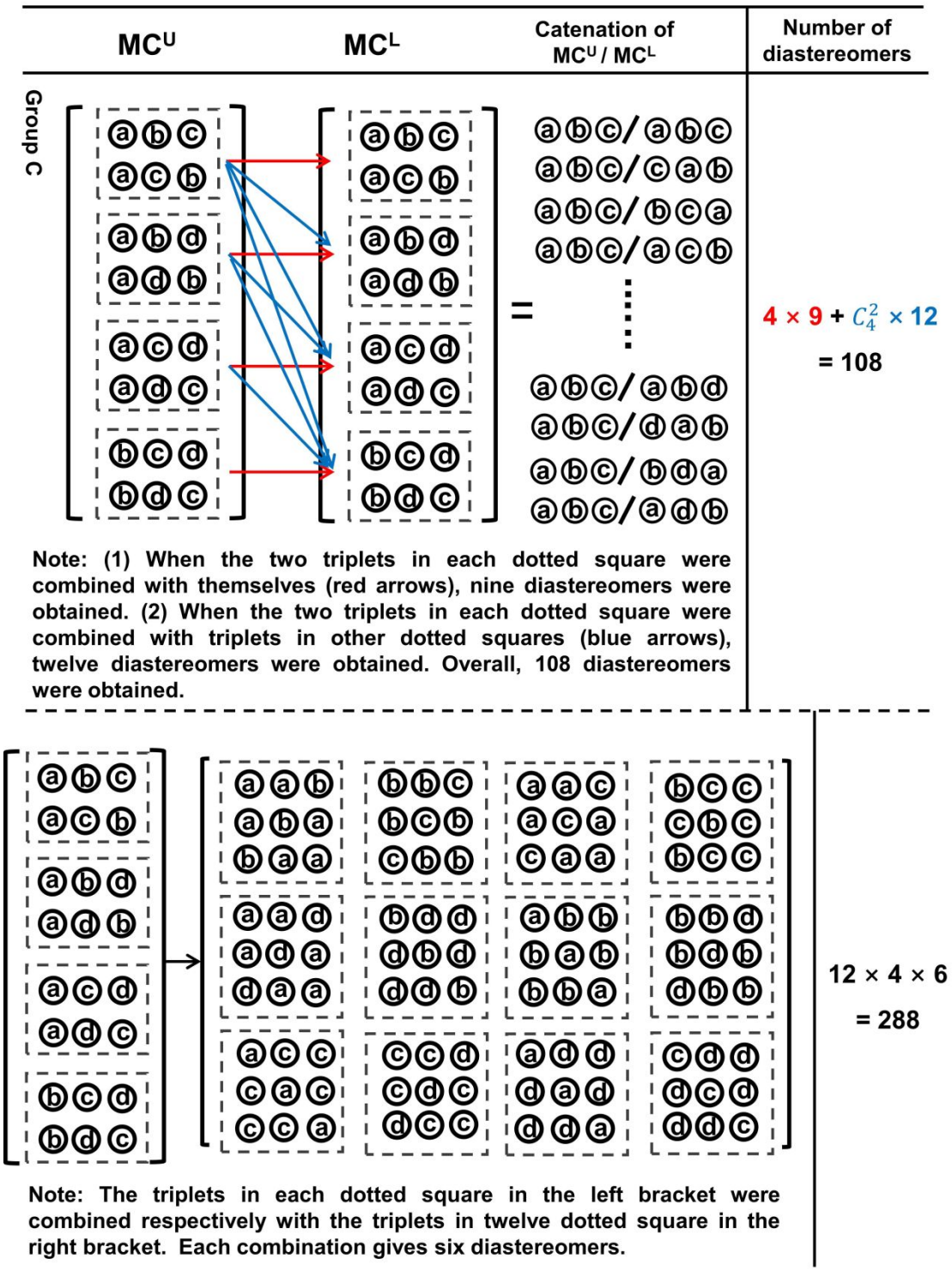
MC^U
MC^L
Catenation of MC^U / MC^L
Number of diastereomers
Group C
abc acb
abd adb
acd adc
bcd bdc
=
abc/abc
abc/cab
abc/bca
abc/acb
abc/abd
abc/dab
abc/bda
abc/adb
4 × 9 + C_4^2 × 12
= 108
Note: (1) When the two triplets in each dotted square were combined with themselves (red arrows), nine diastereomers were obtained. (2) When the two triplets in each dotted square were combined with triplets in other dotted squares (blue arrows), twelve diastereomers were obtained. Overall, 108 diastereomers were obtained.
aab aba baa
bbc bcb cbb
aac aca caa
bcc cbc bcc
aad ada daa
bdd dbd ddb
abb bab bba
bbd bdb dbb
acc cac cca
ccd cdc dcc
add dad dda
cdd dcd ddc
12 × 4 × 6
= 288
Note: The triplets in each dotted square in the left bracket were combined respectively with the triplets in twelve dotted square in the right bracket. Each combination gives six diastereomers.

6. Chiral HPLC Characterizations

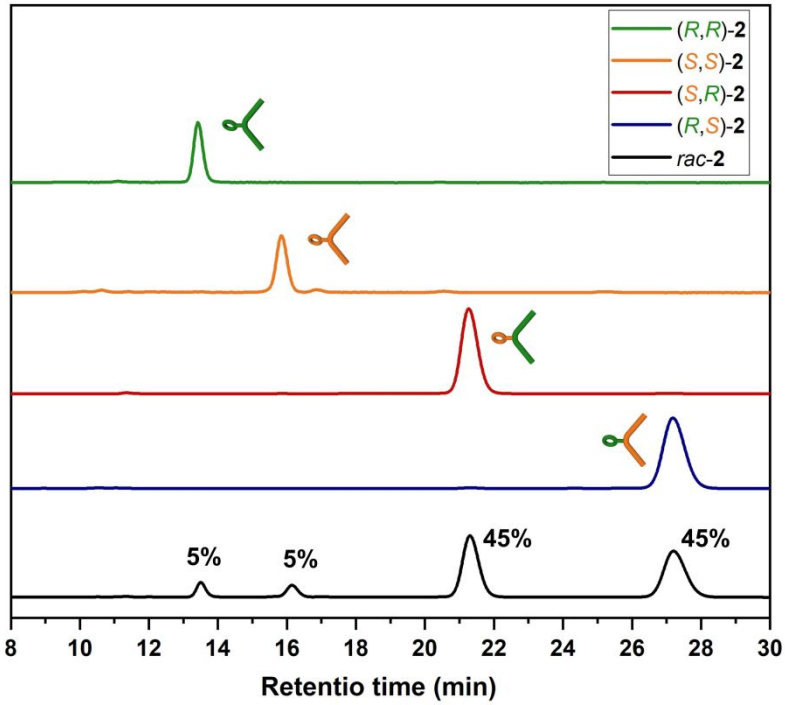

Figure S4. Four enantiopure fractions in *rac*-**2** isolated by preparative HPLC. The enantiopurity of each fraction was further examined by analytical HPLC (detailed HPLC conditions are provided in section **1**), showing satisfactory *ee* value of 96.2% for (***R***, ***R***)-**2**, 94.5% for (***S***, ***S***)-**2**, 99.9% for (***S***, ***R***)-**2** and 99.3% for (***S***, ***R***)-**2**.

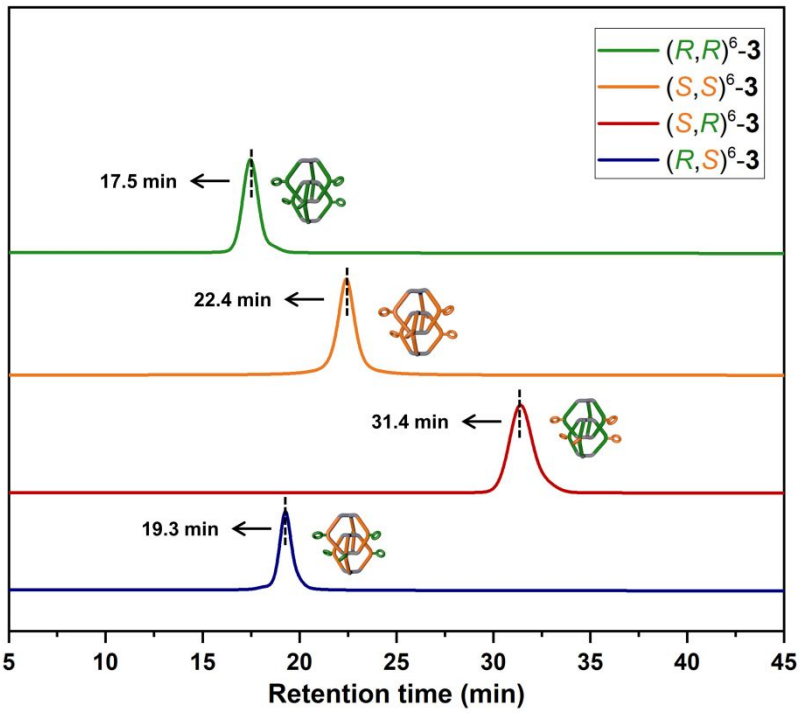

Figure S5. HPLC chromatogram of four homochiral cage-catenanes synthesized separately from corresponding enantiopure precursors (detailed HPLC conditions were provided in section **1**).

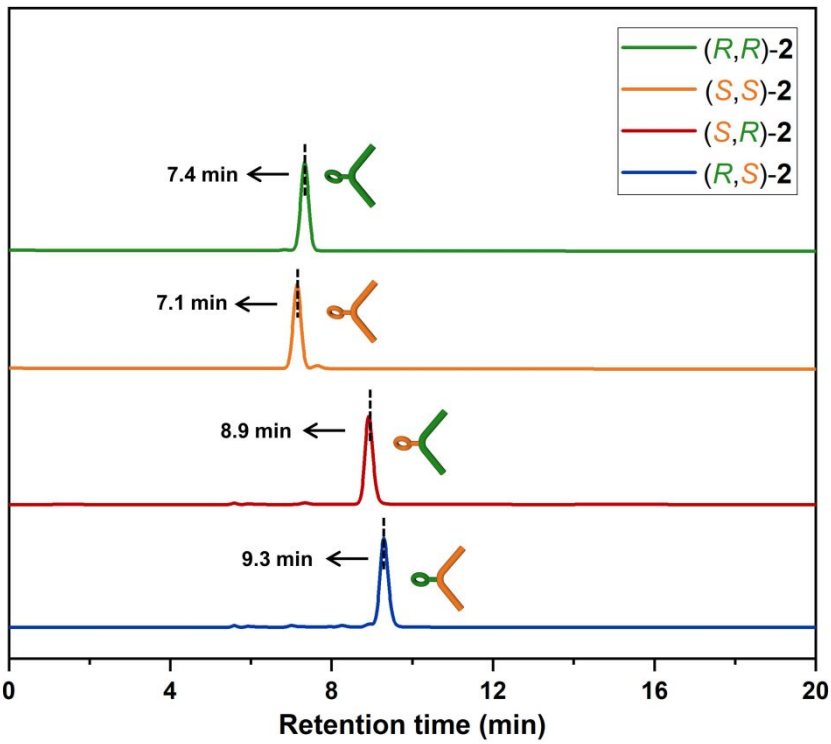

Figure S6. HPLC chromatogram of four chiral linkers under the HPLC conditions of corrresponding homochiral cage-catenanes.

As shown in **Figure S5**, satisfactory separation of four homochiral cage-catenanes were achieved on CHIRALPAK column IA under optimized mobile phase (see Section **1** for details). The corresponding retention time increases in the order of (***R***, ***R***)^6-**3** (17.5 min), (***R***, ***S***)^6-**3** (19.3 min), (***S***, ***S***)^6-**3** (22.4 min) and (***S***, ***R***)^6-**3** (31.4 min).

With an attempt to compare the HPLC sequence of chiral linkers and the resultant cage-catenanes, the retention time of these precursors under the same HPLC conditions were also determined, as shown in **Figure S6**. It turns out that the retention time increases in the order of (***S***, ***S***)-**2** (7.1 min), (***R***, ***R***)-**2** (7.4 min), (***S***, ***R***)-**2** (8.9 min) and (***R***, ***S***)-**2** (9.3 min).

This HPLC sequences variation is tentatively attributed to the configuration change of individual precursors after assembling them into relatively compact cage-catenanes, which might alter their recognition ability with the interaction sites on chiral stationary phases and therefore influence the relative retention time.

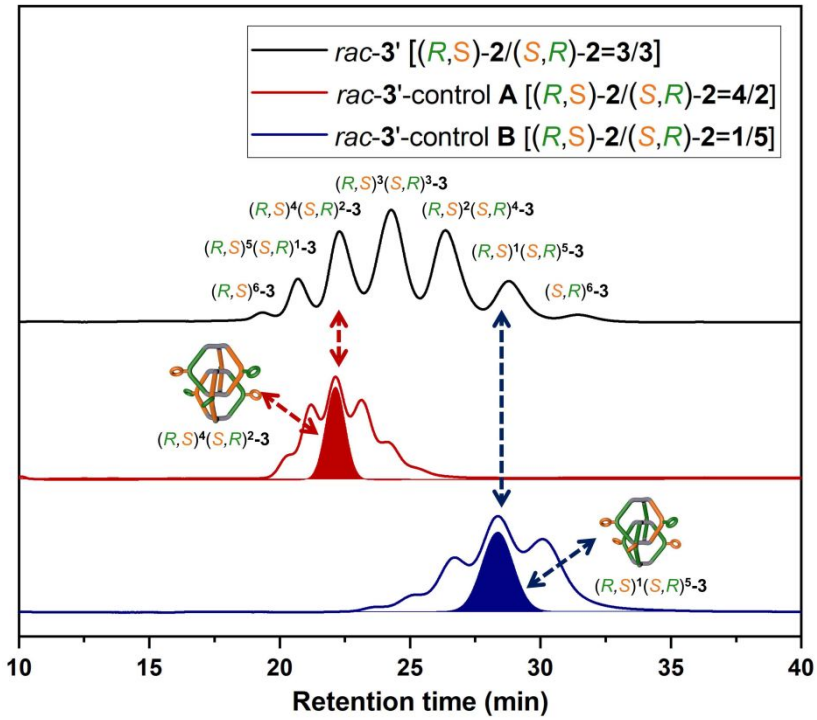

Figure S7. HPLC chromatogram of the purified cage-catenanes synthesized from (***R***, ***S***)**-2** and (***S***, ***R***)**-2** with feed ratio of 4:2 and 1:5, respectiely. The most prominent fraction in the resultant HPLC spectrum should correspond to the isomeric catenane having the same enantiomeric linkers combination as the feed ratio. These control experiments therefore can assist the identification of all the seven frations in *rac*-**3'** (i.e., $(\boldsymbol{R},\boldsymbol{S})^{6-n}(\boldsymbol{S},\boldsymbol{R})^{n}$-**3'**).

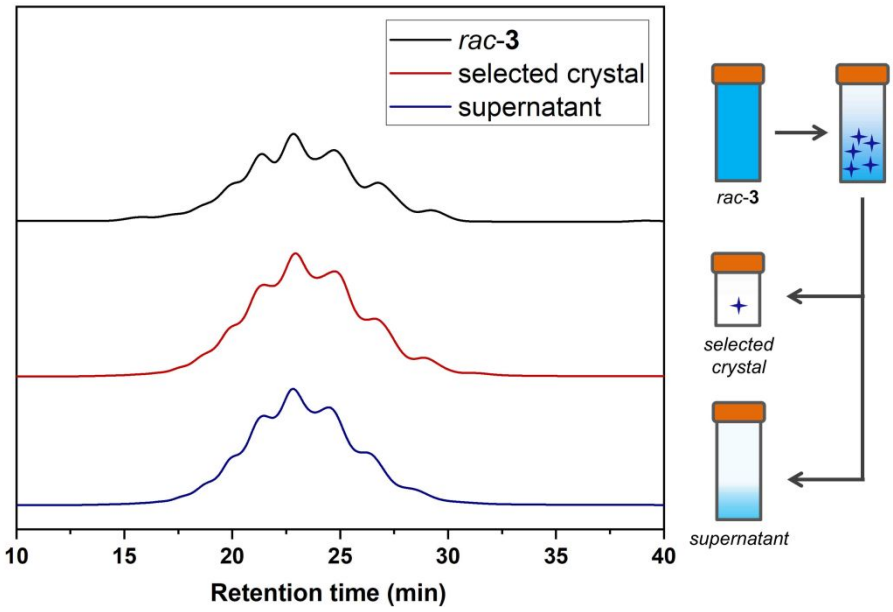

Figure S8. Indiscriminate crystallization of the isomers in *rac*-**3** (i.e., $(\boldsymbol{R},\boldsymbol{R})^{\alpha}(\boldsymbol{S},\boldsymbol{S})^{\beta}(\boldsymbol{S},\boldsymbol{R})^{\gamma}(\boldsymbol{R},\boldsymbol{S})^{\delta}$-**3**). Discrete crystal with relatively bigger size was selected at random, and analyzed again by chiral HPLC after being re-dissolved in chloroform (repeated three times). Representative HPLC spectra of the selected crystal and the supernatant were shown. No discernable change of the diastereomeric composition can be detected among the *rac*-**3**, the selected crystal and supernatant.

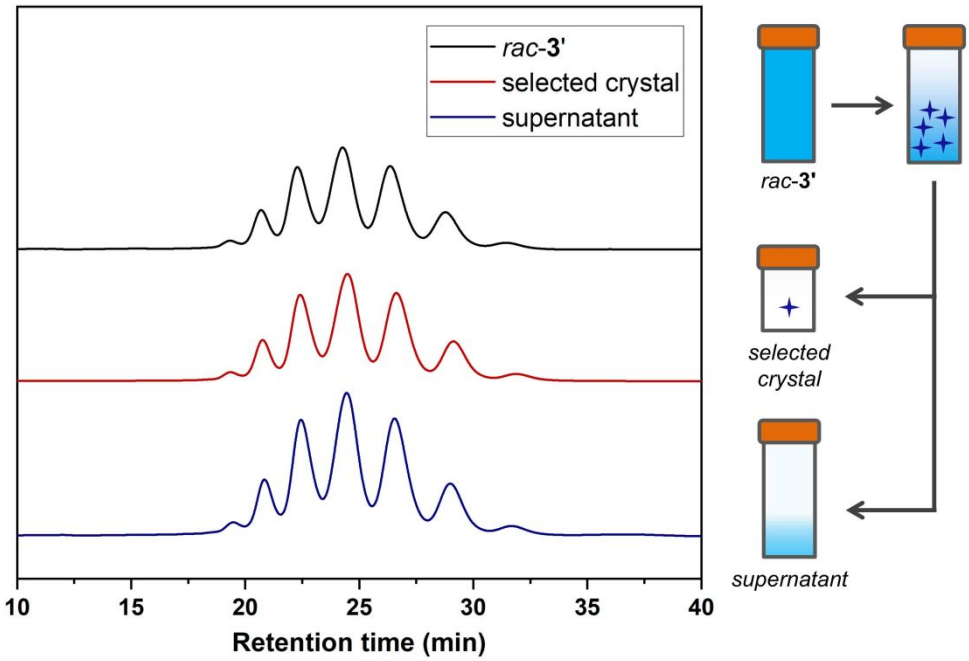

Figure S9. Indiscriminate crystallization of the isomers in *rac*-**3'** (i.e., $(\boldsymbol{R},\boldsymbol{S})^{6-n}(\boldsymbol{S},\boldsymbol{R})^{n}$-**3'**). Discrete crystal with relatively bigger size was selected at random, and analyzed again by chiral HPLC after be re-dissolved in chloroform (repeated three times). Representative HPLC chromatogram of the selected crystal and the left supernatant is shown. No discernable change of the diastereomeric composition can be detected among the *rac*-**3'**, the selected crystal and supernatant.

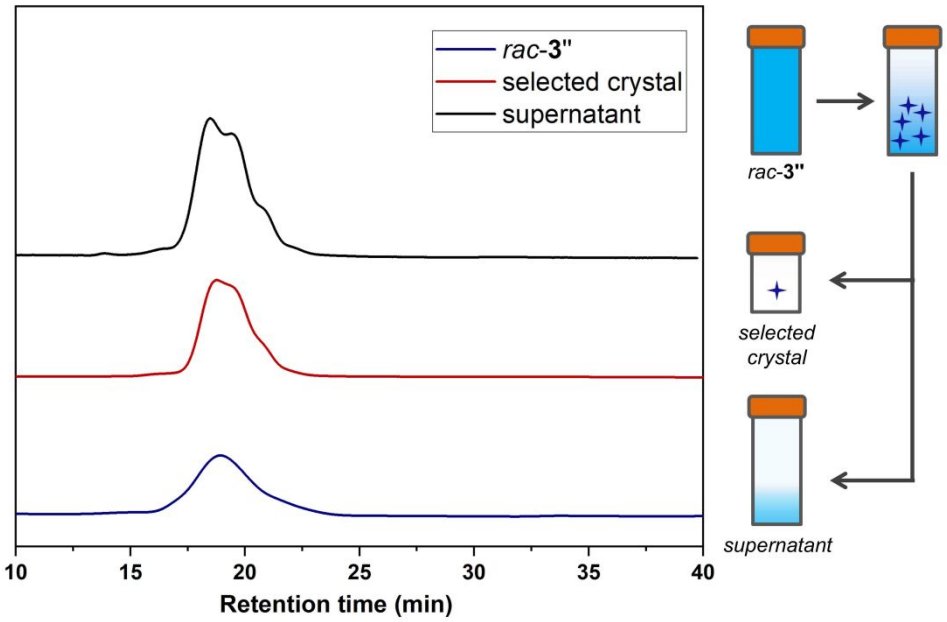

Figure S10. Indiscriminate crystallization of the isomers in *rac*-**3''** (i.e., $(\boldsymbol{R},\boldsymbol{R})^{6-n}(\boldsymbol{S},\boldsymbol{S})^{n}$-**3''**). Discrete crystal with relatively bigger size was selected at random, and analyzed again by chiral HPLC after being re-dissolved in chloroform (repeated three times). Representative HPLC chromatogram of the selected crystal and the supernatant is shown. Only slightly change of the diastereomeric composition can be detected among the *rac*-**3''**, the selected crystal and supernatant.

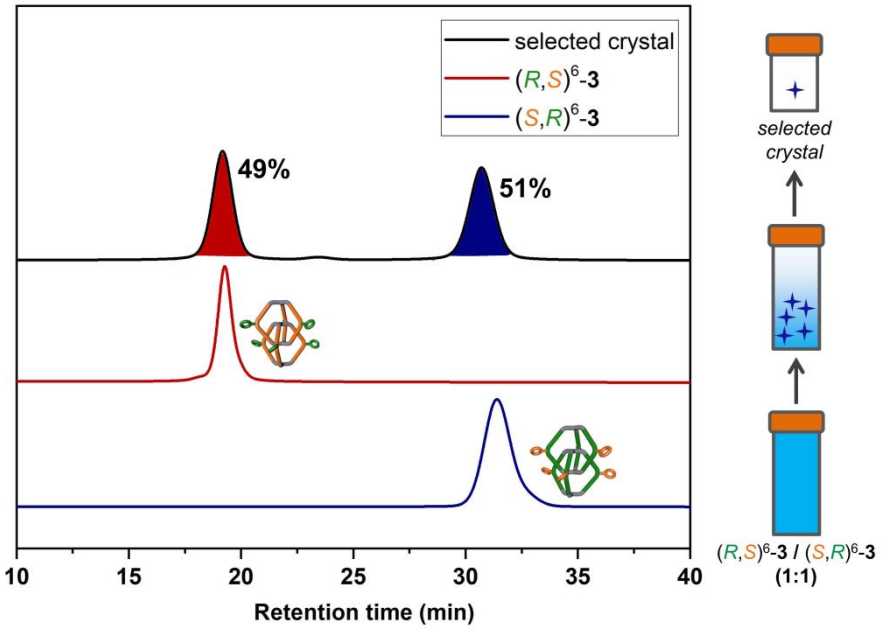

Figure S11. Cocrystallization of the enantiomeric cage-catenane (***S***, ***R***)^6-**3** and (***R***, ***S***)^6-**3** when they were mixed in equal molar ratio. Discrete crystal with relatively bigger size was selected at random, and analyzed again by chiral HPLC after re-dissolving in chloroform (repeated three times). Representative HPLC chromatogram of the selected crystal is shown, presenting two fractions assignable to the standard samples of (***S***, ***R***)^6-**3** and (***R***, ***S***)^6-**3** with nearly equal molar ratio within the tolerant range of experimental error and area intergration.

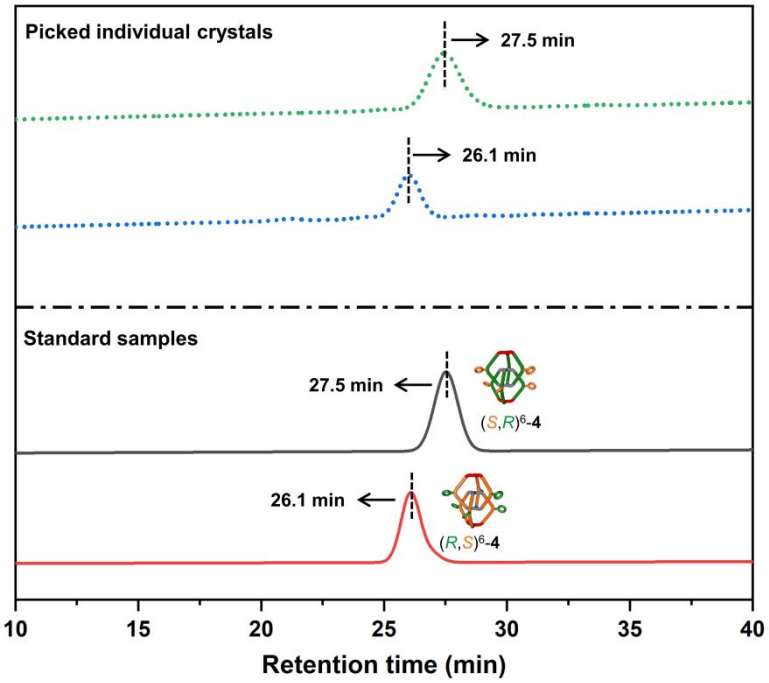

Figure S12. Conglomerate formation of cage-catenane (***S***, ***R***)^6-**4** and (***R***, ***S***)^6-**4** during the crystallization of *rac*-**4** (i.e., (***R***,***R***)$^\alpha$(***S***,***S***)$^\beta$(***S***,***R***)$^\gamma$(***R***,***S***)$^\delta$-**4**). Discrete crystals were selected at random, and analyzed again by chiral HPLC after re-dissolving in tetrahydrofuran (repeated three times). Typical HPLC chromatogram of the picked crystals is shown (dotted lines), presenting individual fraction assignable respectively to the standard samples of (***S***, ***R***)^6-**4** or (***R***, ***S***)^6-**4**.

7. X-Ray Crystallography

Single crystals of (***S***, ***R***)^6-**3** suitable for X-ray crystallography were obtained by slow vapor diffusion of the solution of (***S***, ***R***)^6-**3** in mixed solvents of hexanes and tetrahydrofuran (v:v = 1:1). CCDC deposition number 2099198.

Table S2. Crystal data and structure refinement for (***S***, ***R***)^6-**3**

Identification code	(***S***, ***R***)^6-**3**
Empirical formula	$C_{87}H_{72}N_6S_6$
Formula weight	1393.86
Temperature	170 K
Wavelength	1.34139 Å
Crystal system, space group	Monoclinic, *C*2
Unit cell dimensions	a = 23.095 (2) Å, α = 90°
	b = 31.218 (3) Å, β = 98.485°
	c = 27.692 (3) Å, γ = 90°
Volume	19748 Å^3
Z, Calculated density	8, 0.938 g/cm^3
Absorption coefficient	1.020 mm^{-1}
F (000)	5856
Crystal size	0.1× 0.08 × 0.08 mm^3
Theta range for data collection	2.853° to 55.741°
Limiting indices	-27 <= h <= 27, -37 <= k <= 38, -33 <= l <= 33
Reflections collected	157042
Independent reflections	37560 [$R_{(int)}$ = 0.0870]
Completeness to theta = 53.594	99.8 %
Absorption correction	None
Max and min. transmission	0.7508 and 0.5157
Refinement method	Full-matrix least-squares on F^2
Data / restraints / parameters	37560/944/1514
Goodness-of-fit on F^2	1.204
Final R indices [I>2 sigma (I)]	R1 = 0.1420, wR2 = 0.3481
R indices (all data)	R1 = 0.2082, wR2 = 0.3945
Extinction coefficient	n/a
Largest diff. peak and hole	0.659 and -0.606 e.A^{-3}
Flack parameter	0.41 (2)

Single crystals of (***R***, ***S***)^6-**3** suitable for X-ray crystallography were obtained by slow vapor diffusion of the solution of (***R***, ***S***)^6-**3** in mixed solvents of hexanes and tetrahydrofuran (v:v = 1:1). CCDC deposition number 2099190.

Table S3. Crystal data and structure refinement for (***R***, ***S***)^6-**3**

Identification code	(***R***, ***S***)^6-**3**
Empirical formula	$C_{87}H_{72}N_6S_6$
Formula weight	1393.86
Temperature	170 K
Wavelength	1.34139 Å
Crystal system, space group	Monoclinic, *C*2
Unit cell dimensions	a = 23.0283 (11) Å, α = 90°
	b = 31.0308 (15) Å, β = 98.742°
	c = 27.6059 (14) Å, γ = 90°
Volume	19497.4 Å^3
Z, Calculated density	8, 0.95 g/cm^3
Absorption coefficient	1.033 mm^{-1}
F (000)	5856
Crystal size	0.1× 0.09 × 0.08 mm^3
Theta range for data collection	3.457° to 55.075°
Limiting indices	-28 <= h <= 28, -37 <= k <= 37, -33 <= l <= 33
Reflections collected	116694
Independent reflections	36855 [$R_{(int)}$ = 0.0522]
Completeness to theta = 53.594	99.1 %
Absorption correction	Semi-empirical from equivalents
Max and min. transmission	0.7508 and 0.5642
Refinement method	Full-matrix least-squares on F^2
Data / restraints / parameters	36855/605/1561
Goodness-of-fit on F^2	1.203
Final R indices [I>2 sigma (I)]	R1 = 0.1609, wR2 = 0.3795
R indices (all data)	R1 = 0.2171, wR2 = 0.4155
Extinction coefficient	n/a
Largest diff. peak and hole	0.65 and -0.31 e.A^{-3}
Flack parameter	0.374 (12)

Single crystals of (***R***, ***R***)^6-**3** suitable for X-ray crystallography were obtained by slow vapor diffusion of the solution of (***R***, ***R***)^6-**3** in mixed solvents of hexanes and tetrahydrofuran (v:v = 1:1). CCDC deposition number 2099323.

Table S4. Crystal data and structure refinement for (***R***, ***R***)^6-**3**

Identification code	(***R***, ***R***)^6-**3**
Empirical formula	$C_{87}H_{72}N_6S_6$
Formula weight	1393.86
Temperature	170 K
Wavelength	1.34139 Å
Crystal system, space group	Monoclinic, $P2_1$
Unit cell dimensions	a = 22.0982 (6) Å, α = 90°
	b = 62.5532 (15) Å, β = 94.7025°
	c = 28.0682 (7) Å, γ = 90°
Volume	38668.4 Å^3
Z, Calculated density	16, 0.958 g/cm^3
Absorption coefficient	1.042 mm^{-1}
F (000)	11712
Crystal size	0.18× 0.1 × 0.05 mm^3
Theta range for data collection	2.954° to 55.218°
Limiting indices	-26 <= h <= 23, -76 <= k <= 76, -34 <= l <= 34
Reflections collected	390657
Independent reflections	146254 [$R_{(int)}$ = 0.1082]
Completeness to theta = 53.594	99.7 %
Absorption correction	Semi-empirical from equivalents
Max and min. transmission	0.7508 and 0.4998
Refinement method	Full-matrix least-squares on F^2
Data / restraints / parameters	146254/2381/6399
Goodness-of-fit on F^2	1.308
Final R indices [I>2 sigma (I)]	R1 = 0.1748, wR2 = 0.3901
R indices (all data)	R1 = 0.2715, wR2 = 0.4355
Extinction coefficient	n/a
Largest diff. peak and hole	1.007 and -1.016 e.A^{-3}
Flack parameter	0.333 (9)

Single crystals of (***S***, ***S***)^6-**3** suitable for X-ray crystallography were obtained by slow vapor diffusion of the solution of (***S***, ***S***)^6-**3** in mixed solvents of hexanes and tetrahydrofuran (v:v = 1:1). CCDC deposition number 2099290.

Table S5. Crystal data and structure refinement for (***S***, ***S***)^6-**3 • 0.5THF**

Identification code	(***S***, ***S***)^6-**3 • 0.5THF**
Empirical formula	$C_{89}H_{76}N_6O_{0.5}S_6$
Formula weight	1429.91
Temperature	193 K
Wavelength	1.34139 Å
Crystal system, space group	Monoclinic, $P2_1$
Unit cell dimensions	a = 22.0419 (7) Å, α = 90°
	b = 62.3913 (18) Å, β = 98.477°
	c = 28.1809 (9) Å, γ = 90°
Volume	38637 Å^3
Z, Calculated density	16, 0.983 g/cm^3
Absorption coefficient	1.052 mm^{-1}
F (000)	12032
Crystal size	0.18× 0.1 × 0.05 mm^3
Theta range for data collection	2.954° to 55.191°
Limiting indices	-26 <= h <= 26, -76 <= k <= 76, -34 <= l <= 34
Reflections collected	404037
Independent reflections	146788 [$R_{(int)}$ = 0.0881]
Completeness to theta = 53.594	99.8 %
Absorption correction	Semi-empirical from equivalents
Max and min. transmission	0.7508 and 0.4850
Refinement method	Full-matrix least-squares on F^2
Data / restraints / parameters	146788/95/7321
Goodness-of-fit on F^2	1.040
Final R indices [I>2 sigma (I)]	R1 = 0.1022, wR2 = 0.2730
R indices (all data)	R1 = 0.1395, wR2 = 0.3119
Extinction coefficient	n/a
Largest diff. peak and hole	1.245 and -0.482 e.A^{-3}
Flack parameter	0.199 (5)

Single crystals of *mix*-**3** suitable for X-ray crystallography were obtained by slow vapor diffusion of the solution of *mix*-**3** in mixed solvents of hexanes and tetrahydrofuran (v:v = 1:1). CCDC deposition number 2105275.

Table S6. Crystal data and structure refinement for *mix*-**3**

Identification code	*mix*-**3**
Empirical formula	$C_{87}H_{72}N_6S_6$
Formula weight	1393.86
Temperature	170 K
Wavelength	1.34139 Å
Crystal system, space group	Monoclinic, *C*2/c
Unit cell dimensions	a = 22.9243 (7) Å, α = 90°
	b = 31.1943 (18) Å, β = 98.5278°
	c = 27.6944 (9) Å, γ = 90°
Volume	19585.5 $Å^3$
Z, Calculated density	8, 0.945 g/cm^3
Absorption coefficient	1.029 mm^{-1}
F (000)	5856
Crystal size	0.08× 0.06 × 0.06 mm^3
Theta range for data collection	3.296° to 49.654°
Limiting indices	-26 <= h <= 25, -34 <= k <= 35, -31 <= l <= 31
Reflections collected	92634
Independent reflections	14617 [$R_{(int)}$ = 0.1132]
Completeness to theta = 53.594	97.2 %
Absorption correction	Semi-empirical from equivalents
Max and min. transmission	0.7508 and 0.3732
Refinement method	Full-matrix least-squares on F^2
Data / restraints / parameters	14617/491/808
Goodness-of-fit on F^2	1.114
Final R indices [I>2 sigma (I)]	R1 = 0.1830, wR2 = 0.3704
R indices (all data)	R1 = 0.2850, wR2 = 0.4238
Extinction coefficient	n/a
Largest diff. peak and hole	0.556 and -0.343 $e.A^{-3}$

Single crystals of (***S***, ***R***)^6-**4** suitable for X-ray crystallography were obtained by slow vapor diffusion of the solution of *rac*-**4** in mixed solvents of tetrahydrofuran and acetonitrile (v:v = 5:2). CCDC deposition number 2099313.

Table S7. Crystal data and structure refinement for (***S***, ***R***)^6-**4**

Identification code	(***S***, R)^6-**4**
Empirical formula	$C_{87}H_{78}N_6S_6$
Formula weight	1399.92
Temperature	170 K
Wavelength	1.34139 Å
Crystal system, space group	Trigonal, *R*32
Unit cell dimensions	a = 33.851 (7) Å, α = 90°
	b = 33.851 (7) Å, β = 90°
	c = 14.9517 (4) Å, γ = 120°
Volume	14838 Å^3
Z, Calculated density	6, 0.940 g/cm^3
Absorption coefficient	1.019 mm^{-1}
F (000)	4428
Crystal size	0.1× 0.08 × 0.06 mm^3
Theta range for data collection	2.886° to 55.028°
Limiting indices	-41 <= h <= 41, -30 <= k <= 41, -18 <= l <= 18
Reflections collected	54038
Independent reflections	6279 [$R_{(int)}$ = 0.0643]
Completeness to theta = 53.594	98.3 %
Absorption correction	Semi-empirical from equivalents
Max and min. transmission	0.7508 and 0.4866
Refinement method	Full-matrix least-squares on F^2
Data / restraints / parameters	6279/245/308
Goodness-of-fit on F^2	0.913
Final R indices [I>2 sigma (I)]	R1 = 0.1134, wR2 = 0.2754
R indices (all data)	R1 = 0.1643, wR2 = 0.3114
Extinction coefficient	n/a
Largest diff. peak and hole	0.260 and -0.215 e.A^{-3}
Flack parameter	0.171 (17)

Single crystals of (***R***, ***S***)^6-**4** suitable for X-ray crystallography were obtained by slow vapor diffusion of the solution of *rac*-**4** in mixed solvents of tetrahydrofuran and acetonitrile (v:v = 5:2). CCDC deposition number 2099293.

Table S8. Crystal data and structure refinement for (***R***, ***S***)^6-**4** • **3**MeCN

Identification code	(***R***, ***S***)^6-**4** • **3**MeCN
Empirical formula	$C_{180}H_{165}N_{15}S_{12}$
Formula weight	2922.92
Temperature	170 K
Wavelength	1.34139 Å
Crystal system, space group	Trigonal, *R*32
Unit cell dimensions	a = 33.8271 (7) Å, α = 90°
	b = 33.8271 (7) Å, β = 90°
	c = 14.8818 (4) Å, γ = 120°
Volume	14747.4 Å^3
Z, Calculated density	3, 0.987 g/cm^3
Absorption coefficient	1.051 mm^{-1}
F (000)	4626
Crystal size	0.2× 0.18 × 0.16 mm^3
Theta range for data collection	3.938° to 55.123°
Limiting indices	-41 <= h <= 40, -25 <= k <= 40, -18 <= l <= 18
Reflections collected	52813
Independent reflections	6226 [$R_{(int)}$ = 0.0541]
Completeness to theta = 53.594	98.8 %
Absorption correction	Semi-empirical from equivalents
Max and min. transmission	0.7508 and 0.4712
Refinement method	Full-matrix least-squares on F^2
Data / restraints / parameters	6226/224/303
Goodness-of-fit on F^2	0.847
Final R indices [I>2 sigma (I)]	R1 = 0.1309, wR2 = 0.2942
R indices (all data)	R1 = 0.1708, wR2 = 0.3217
Extinction coefficient	n/a
Largest diff. peak and hole	0.324 and -0.222 e.A^{-3}
Flack parameter	0.167 (16)

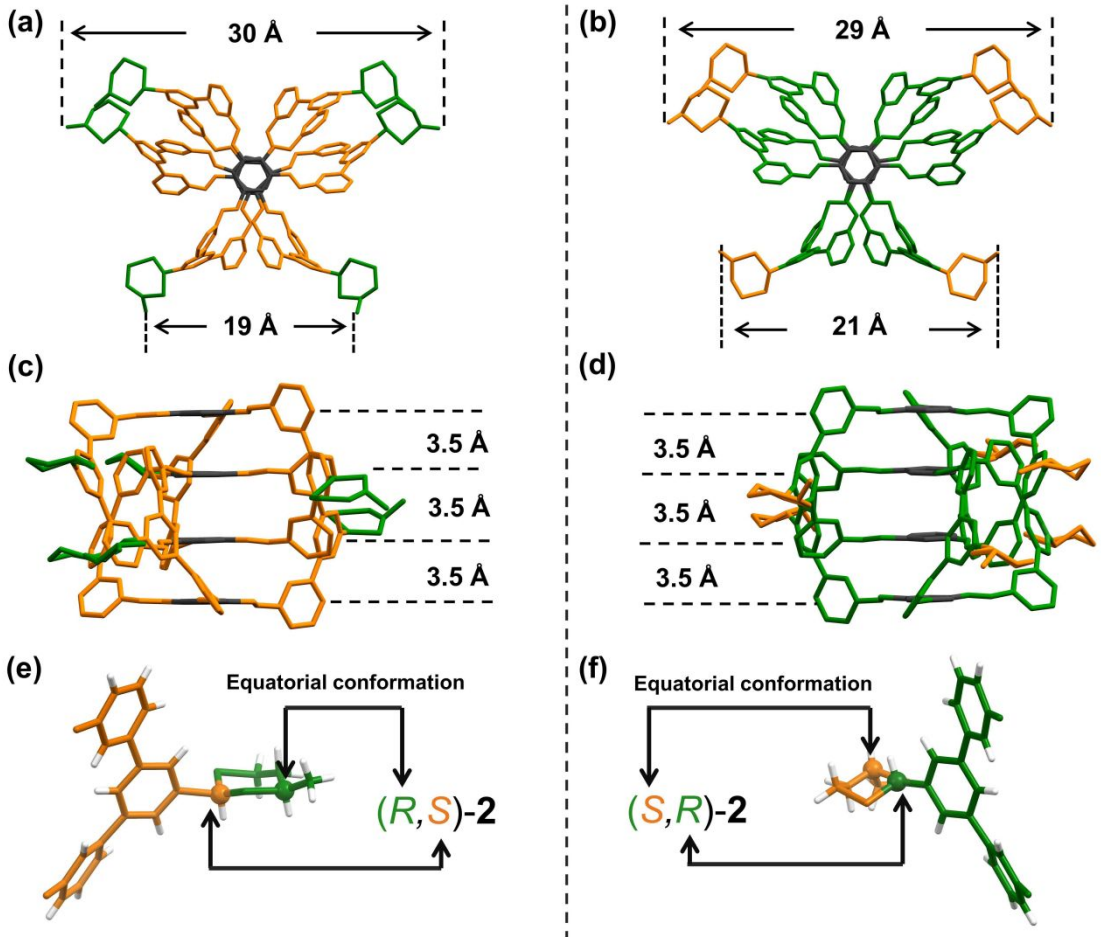

Figure S13. Molecular structures of enantiopure cage-catenanes (***R***, ***S***)^6-**3** and (***S***, ***R***)^6-**3** in single crystals. (a) and (b) Top view of the triply interlocked structure showing the twist of six *m*-terphenyl linkers for both (***R***, ***S***)^6-**3** and (***S***, ***R***)^6-**3**. A butterfly configuration of the terphenyl blades can be visualized, as four linkers stretched symmetrically on one side (spanning a distance of 30 Å) and two linkers on the other side (spanning a distance of ~20 Å). (c) and (d) Side view of (***R***, ***S***)^6-**3** and (***S***, ***R***)^6-**3** showing the vertical stacking of aromatic panels with an interval distance of 3.5 Å. (e) and (f) Truncated *m*-terphenyl linkers from the crystal structure of (***R***, ***S***)^6-**3** and (***S***, ***R***)^6-**3** demonstrating their absolute configurations and the equatorial conformation of the methyl group. Two stereocenters are highlighted in ball and stick mode. The panels, *m*-terphenyl linkers and the lateral dithiane groups are marked in gray, yellow and green, respectively. Hydrogen atoms are only displayed in (e) and (f) to facilitate chirality and configuration determination.

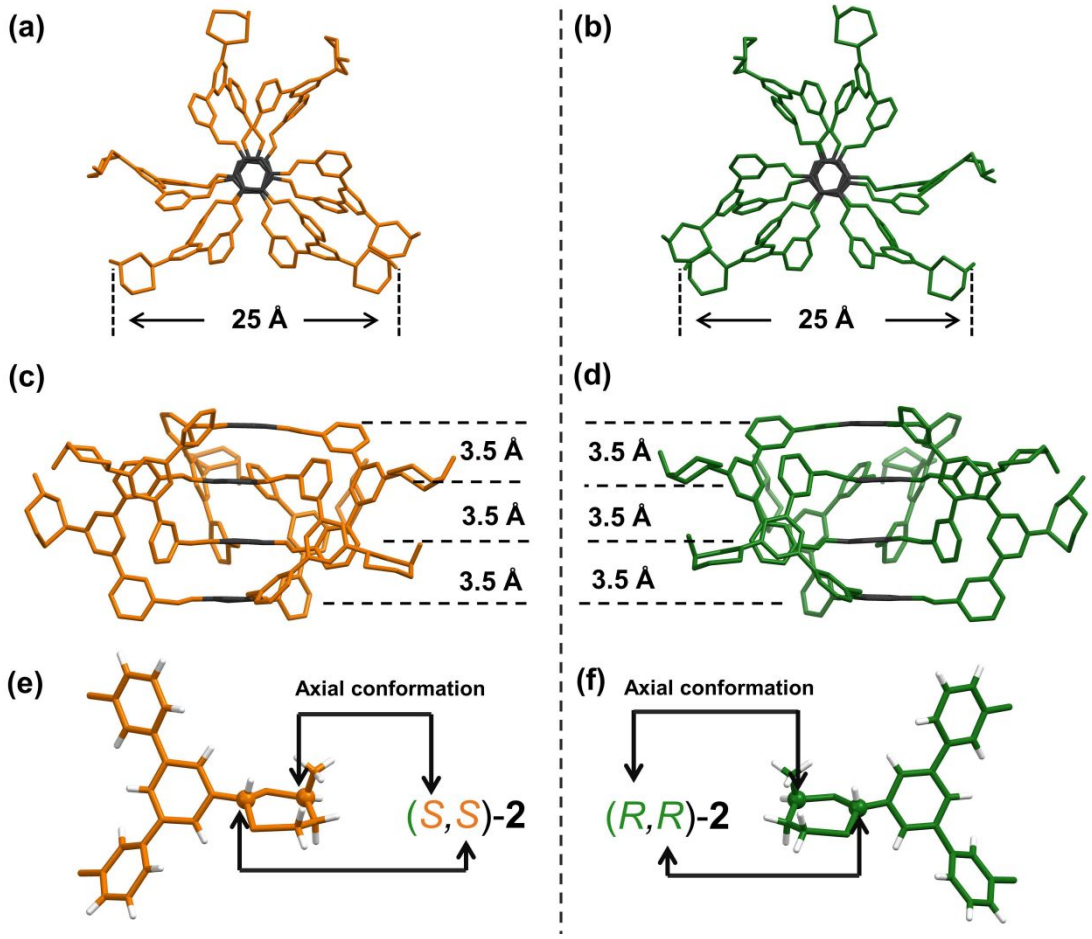

Figure S14. Molecular structures of enantiopure cage-catenanes (***S***, ***S***)^6-**3** and (***R***, ***R***)^6-**3** in single crystals. (a) and (b) Top view of the triply interlocked structure showing the twist of six *m*-terphenyl linkers for both (***S***, ***S***)^6-**3** and (***R***, ***R***)^6-**3**. Aside from the irregular twist of linkers, two lateral dithiane groups are also noticeably distorted probably due to the dense packing during crystallization. (c) and (d) Side view of (***S***, ***S***)^6-**3** and (***R***, ***R***)^6-**3** showing the vertical stacking of aromatic panels with an interval distance of 3.5 Å. (e) and (f) Truncated *m*-terphenyl linkers from the crystal structure of (***S***, ***S***)^6-**3** and (***R***, ***R***)^6-**3** demonstrating their absolute configurations and the axial conformation of the methyl group. Two stereocenters are highlighted in ball and stick mode. The panels, *m*-terphenyl linkers and the lateral dithiane groups are marked in gray, yellow and green, respectively. Hydrogen atoms are only displayed in (e) and (f) to facilitate chirality and configuration determination.

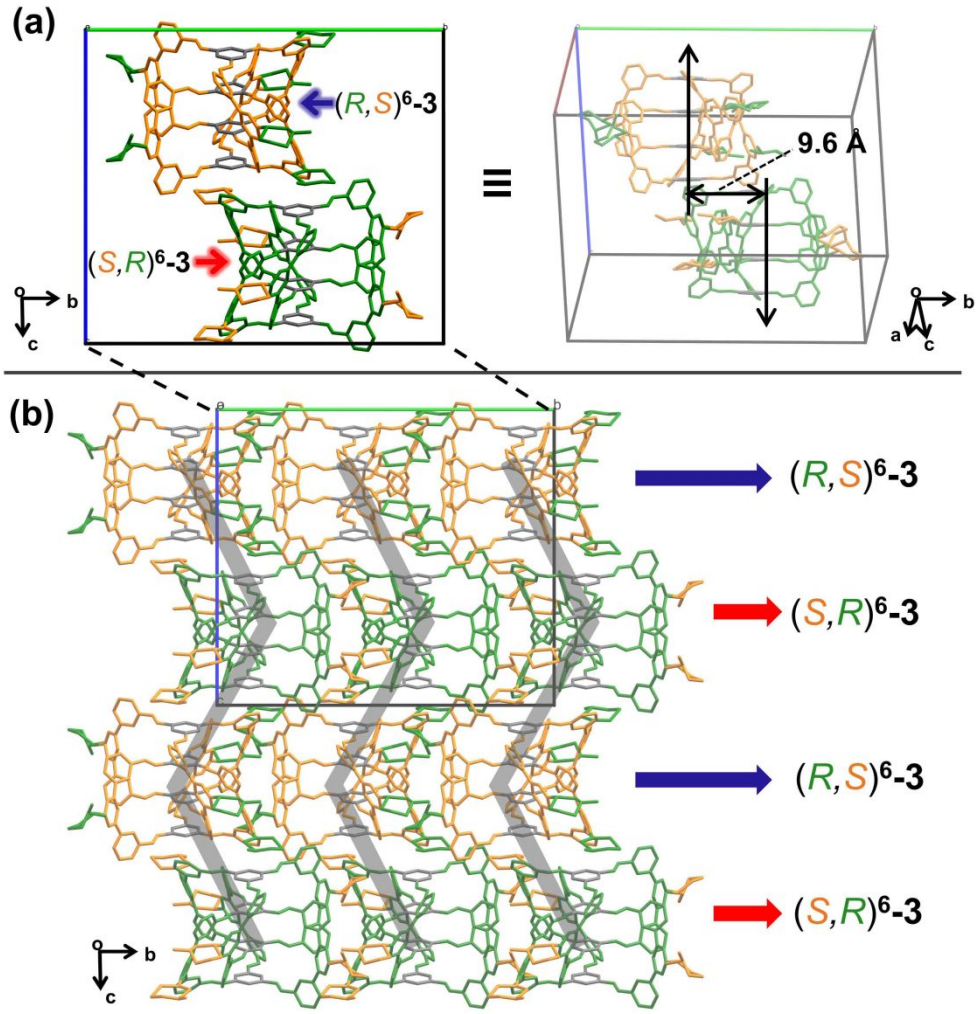

Figure S15. The crystal of a racemic compound formed by a racemic pair of (***R***, ***S***)^6-**3** and (***S***, ***R***)^6-**3**. (a) Discrete crystal consists of an equimolar ratio of both enantiomers (***R***, ***S***)^6-**3** and (***S***, ***R***)^6-**3** in a unit cell. Due to the absence of longitudinal π-π stacking, two neighbouring enantiomers are arranged in a staggered fashion with a lateral offset of 9.6 Å. (b) When viewed along the *c*-axis, enantiomers are aligned alternately in separate rows, leading to a zigzag packing diagram. In this scenario, no directional supramolecular interactons are established because of this less ordered structures.

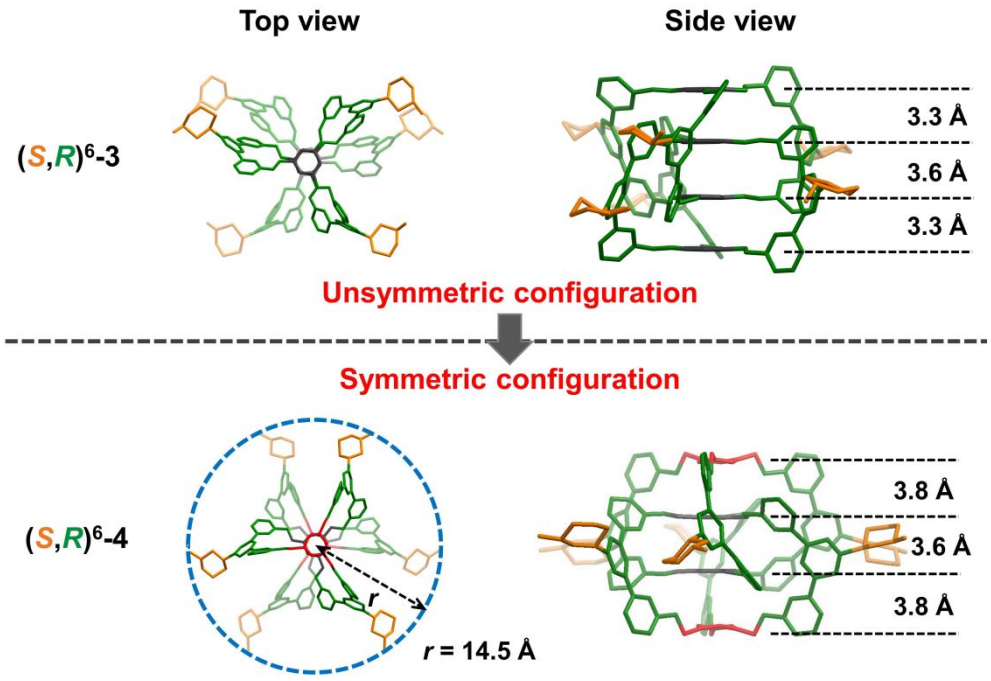

Figure S16. The fully rigid molecular skeleton of cage-catenane (***S***, ***R***)^6-**3** contributes to an unsymmetric configuration of the six *m*-terphenyl blades during crystalline packing. In contrast, cage-catenane (***S***, ***R***)^6-**4** bearing flexible exterior panels adopts a highly symmetric configuration. In both scenarios, triple π-π interaction within the internal panels are observed.

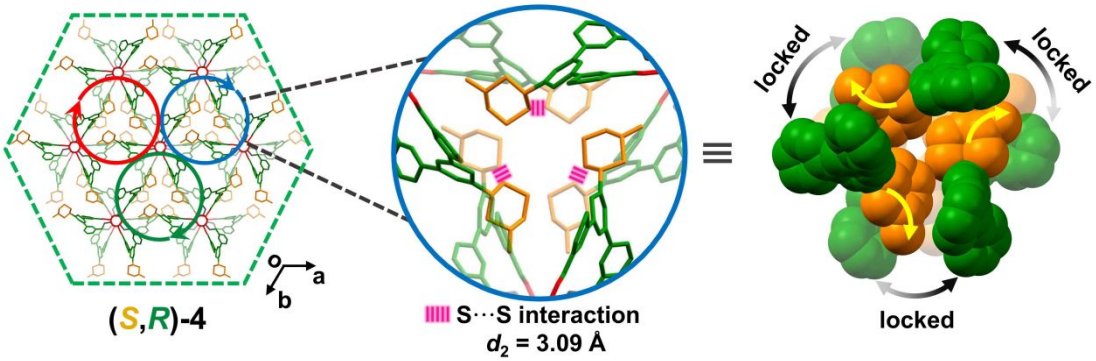

Figure S17. The supramolecular columns of (***S***, ***R***)^6-**4** are associated through their lateral dithiane moieties, forming three adjacent regions with S□□□S close contact. When viewed from *c*-axis, the S□□□S interactions (d_2 = 3.09 Å) between two superimposed dithiane moieties are shown in stick mode by purple dash line. The consecutive locking of dithiane moieties between two adjacent *m*-terphenyl blades are further illustrated in space-filling mode.

8. NMR Spectra of Precursors and Cage-catenanes

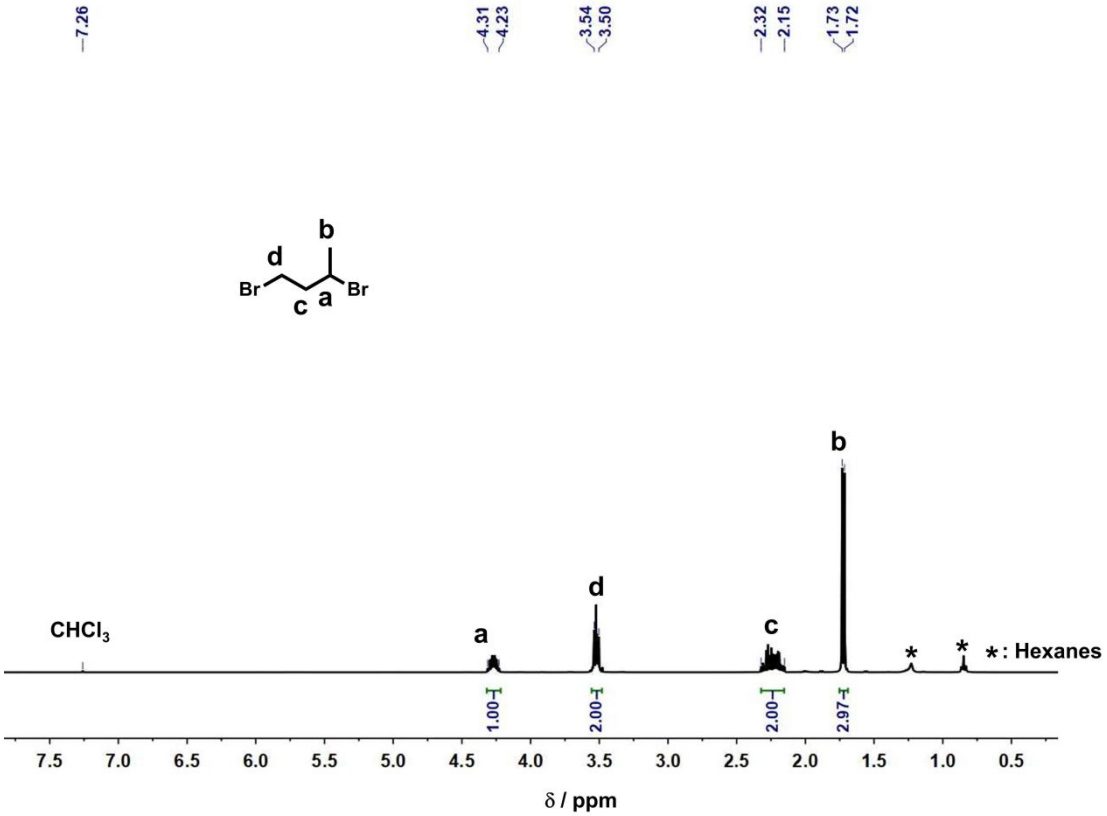

Figure S18. ^{1}H NMR spectrum of 1,3-dibromobutane in $CDCl_3$.

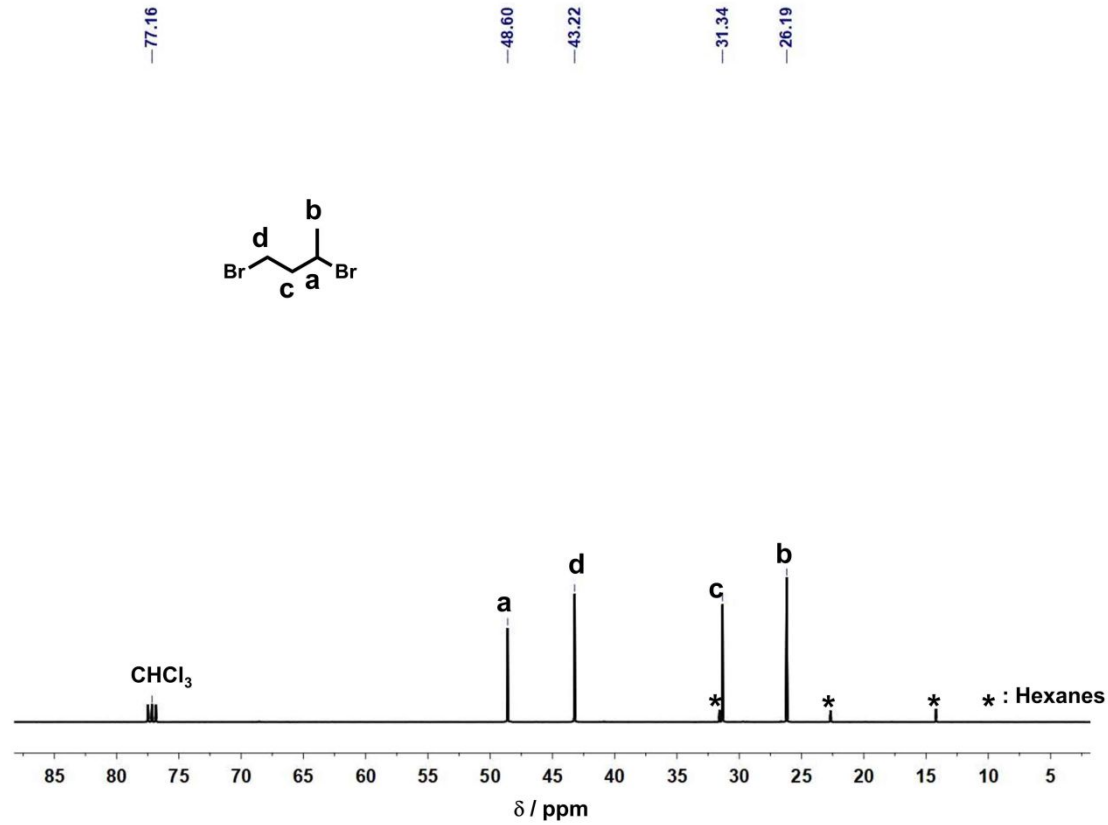

Figure S19. ^{13}C NMR spectrum of 1,3-dibromobutane in $CDCl_3$.

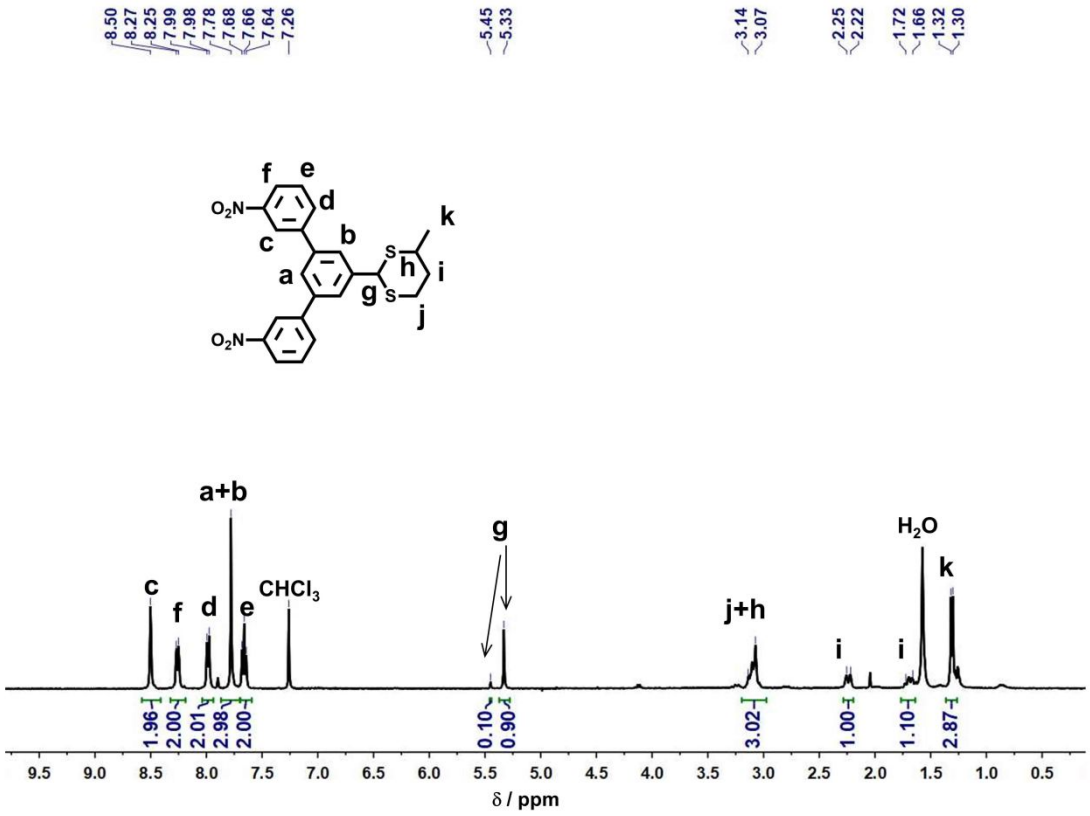

Figure S20. ^{1}H NMR spectrum of *rac*-**DNPMD** in $CDCl_3$.

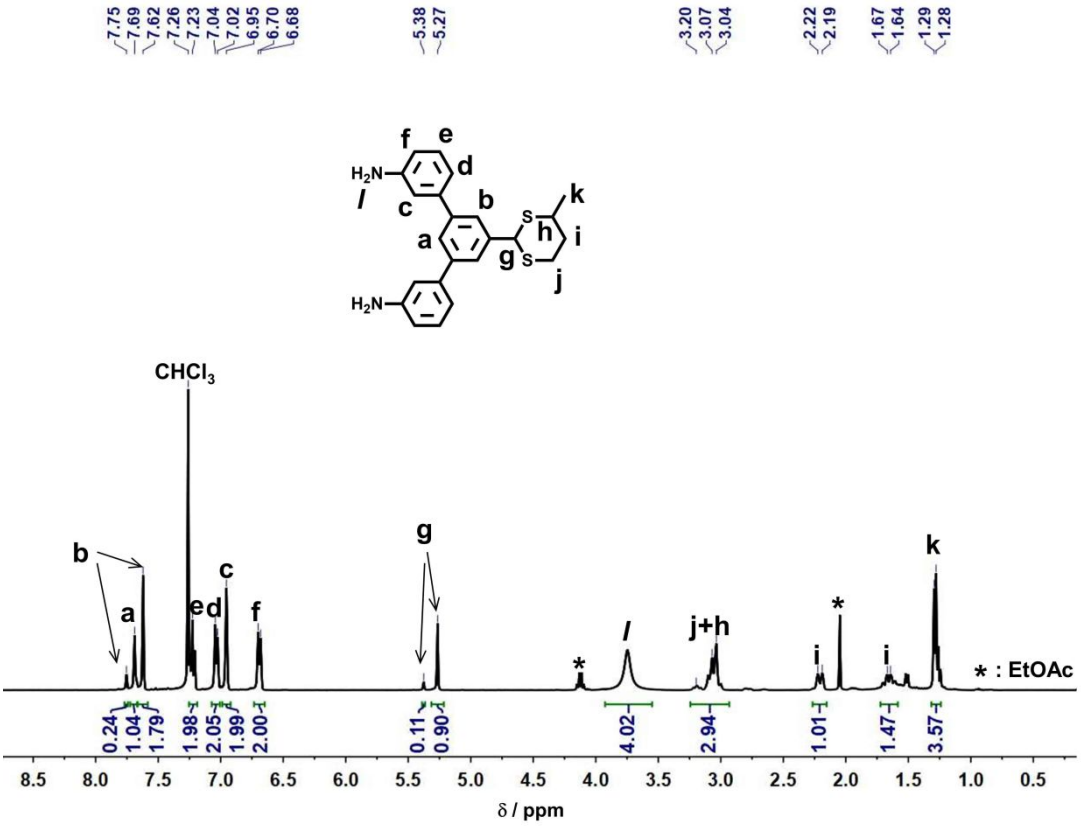

Figure S21. ^{1}H NMR spectrum of *rac*-**2** in $CDCl_3$.

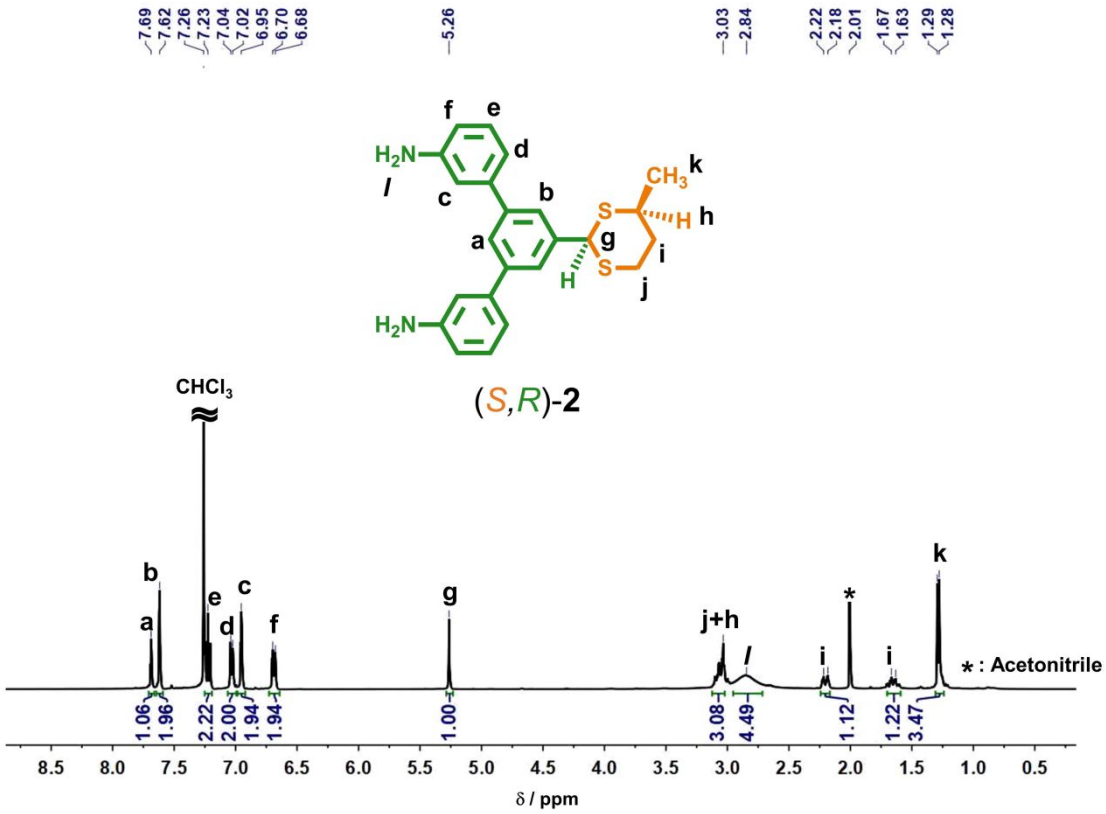

Figure S22. ^{1}H NMR spectrum of (***S***, ***R***)-**2** in $CDCl_3$.

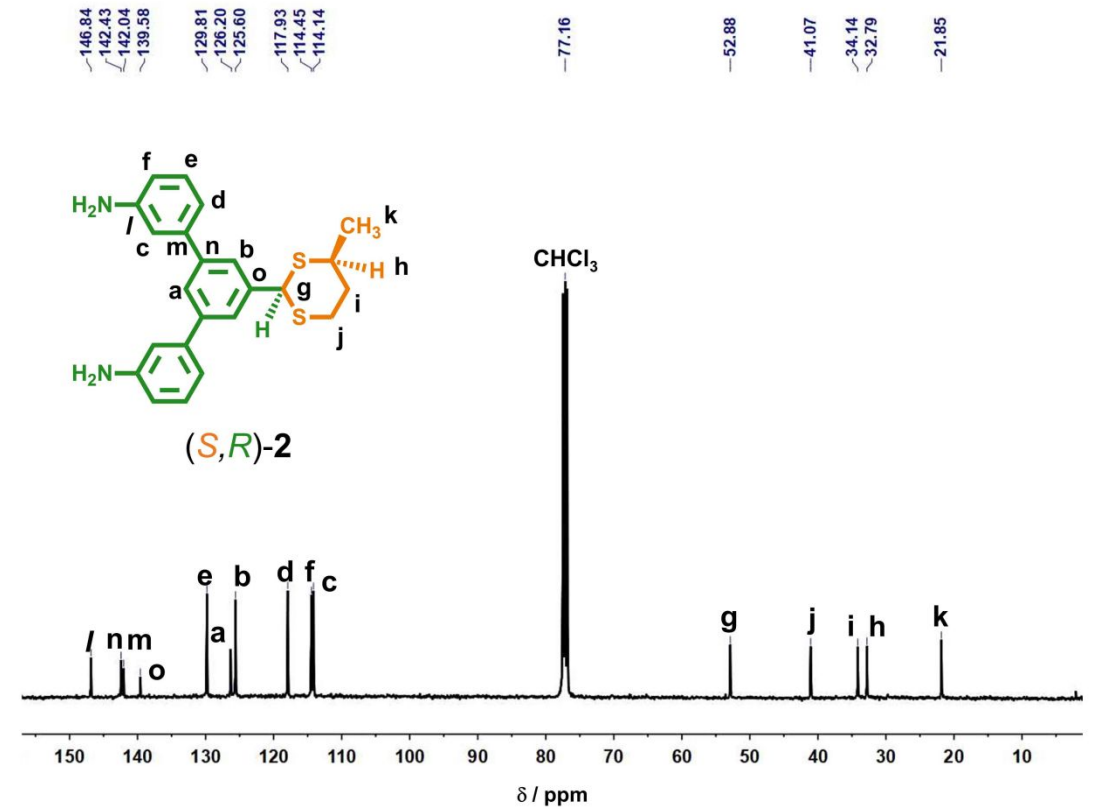

Figure S23. ^{13}C NMR spectrum of (***S***, ***R***)-**2** in $CDCl_3$.

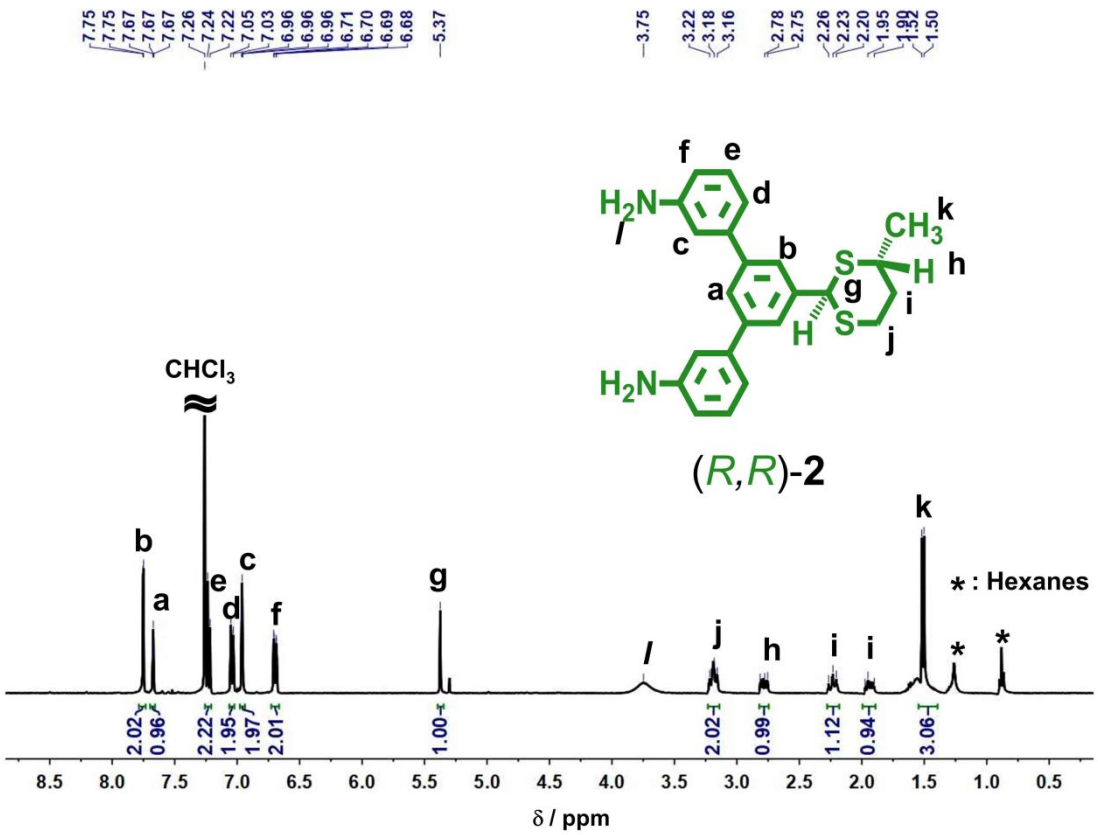

Figure S24. ^{1}H NMR spectrum of (***R***, ***R***)-**2** in $CDCl_3$.

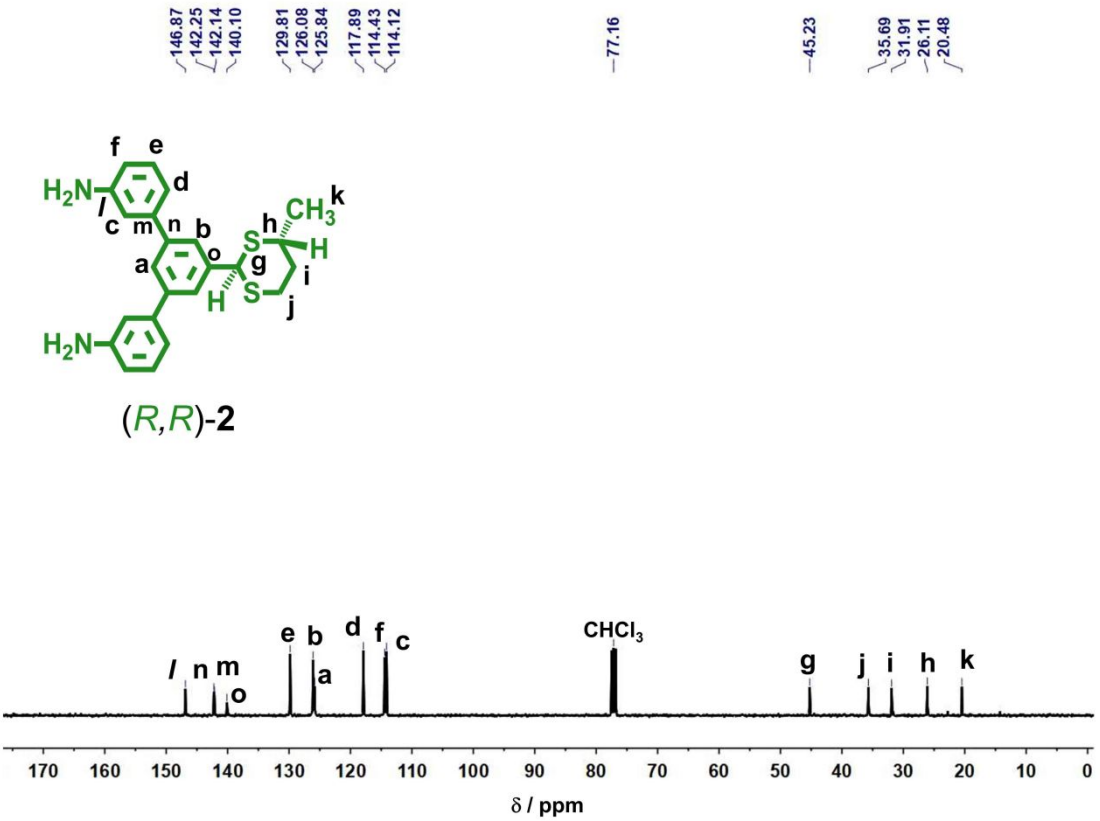

Figure S25. ^{13}C NMR spectrum of (***R***, ***R***)-**2** in $CDCl_3$.

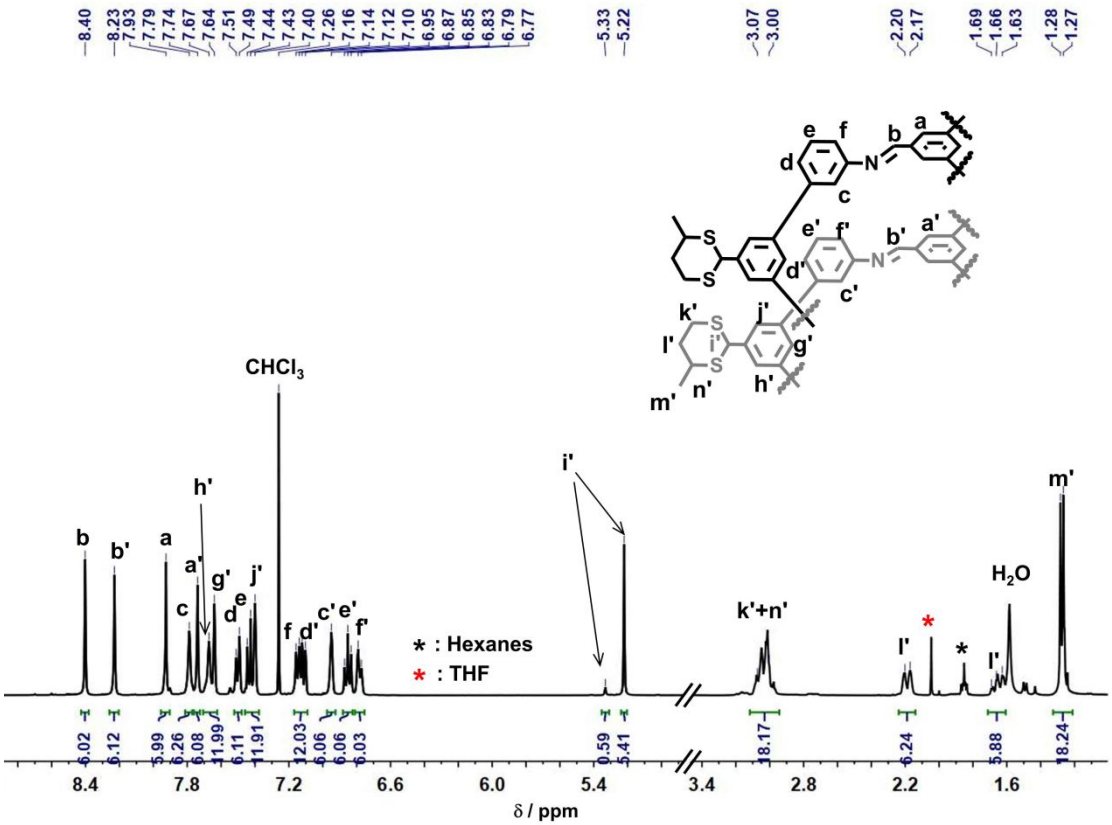

Figure S26. ^{1}H NMR spectrum of *rac*-**3** in $CDCl_3$.

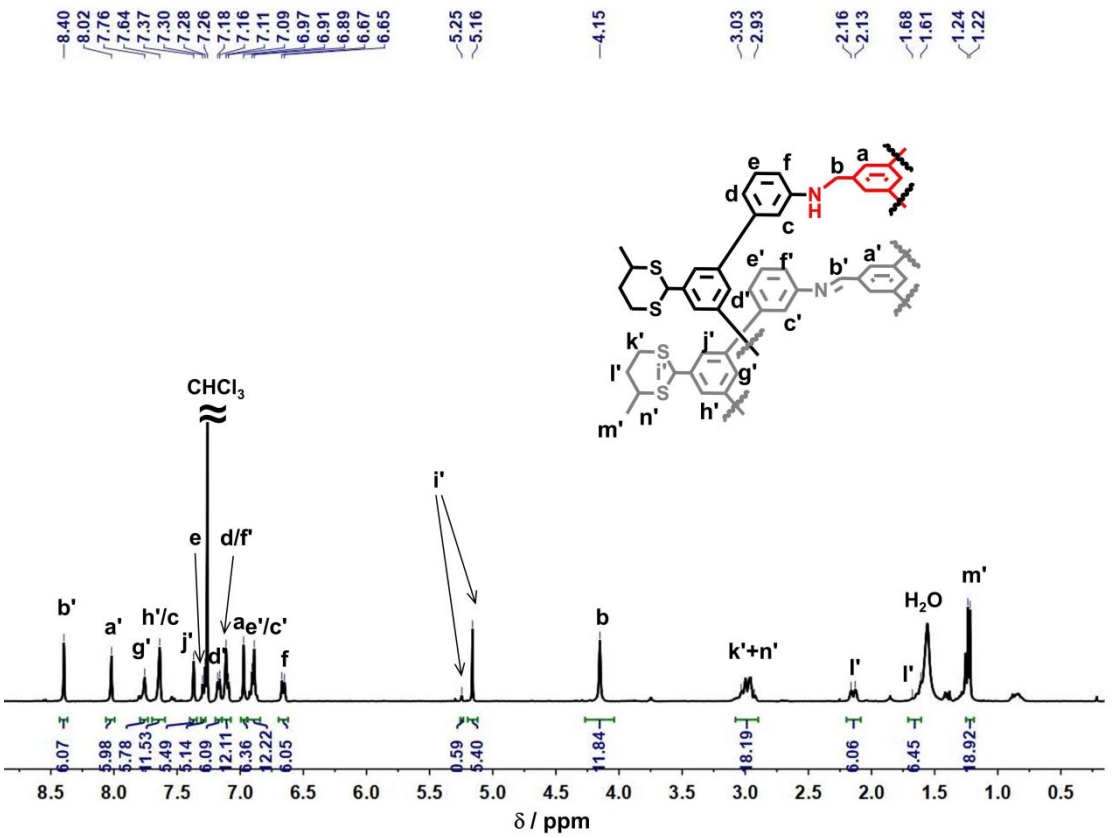

Figure S27. ^{1}H NMR spectrum of *rac*-**4** in $CDCl_3$.

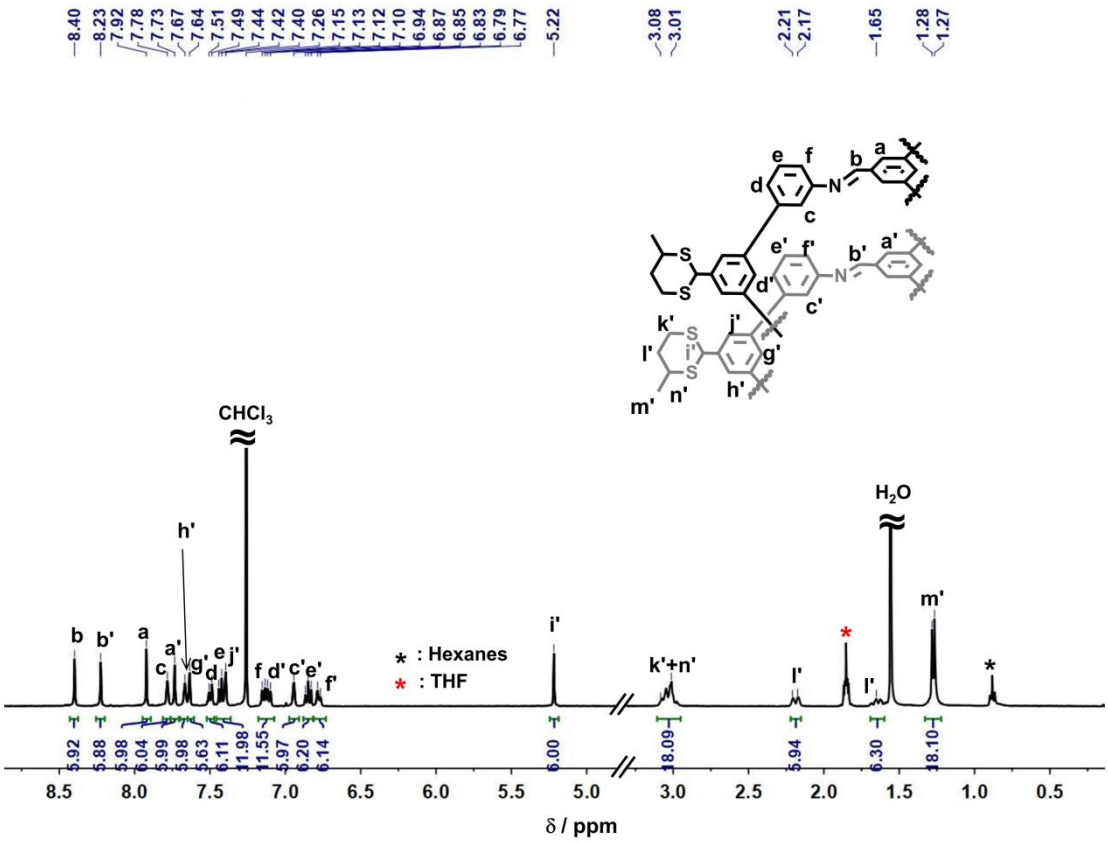

Figure S28. ^{1}H NMR spectrum of *rac*-**3'** in $CDCl_3$.

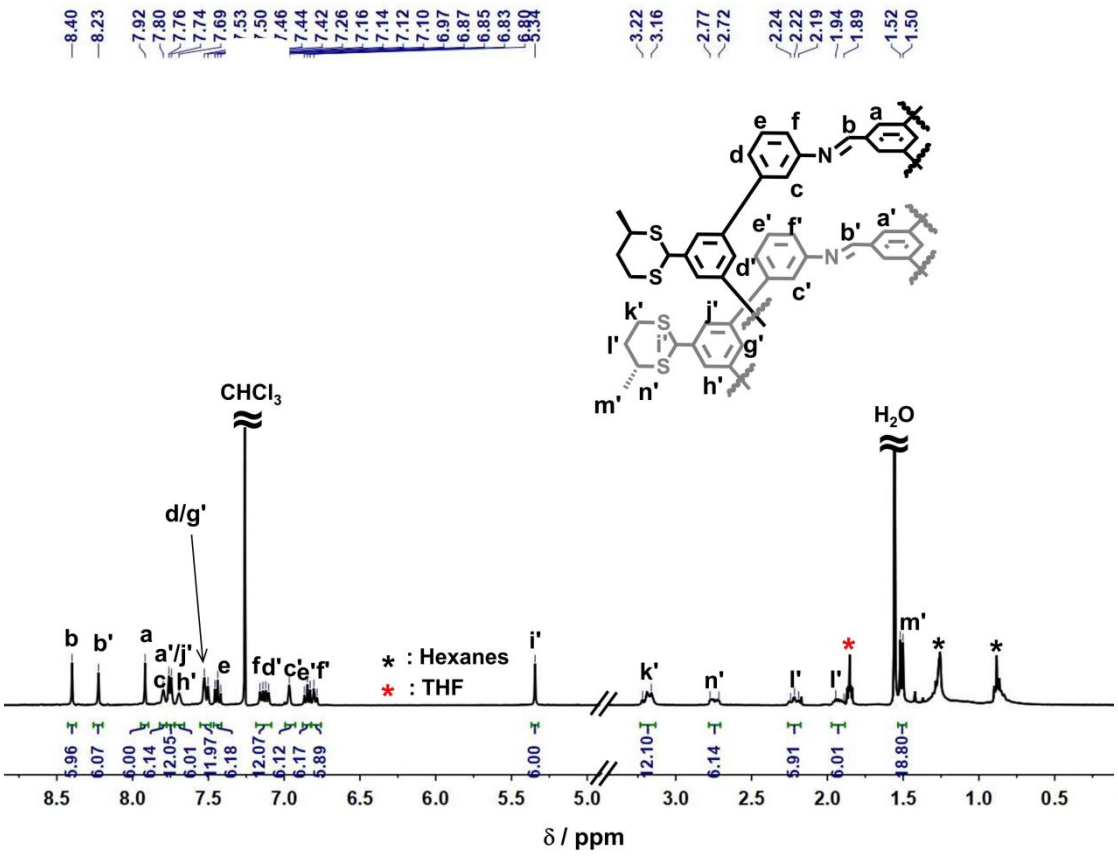

Figure S29. ^{1}H NMR spectrum of *rac*-**3''** in $CDCl_3$.

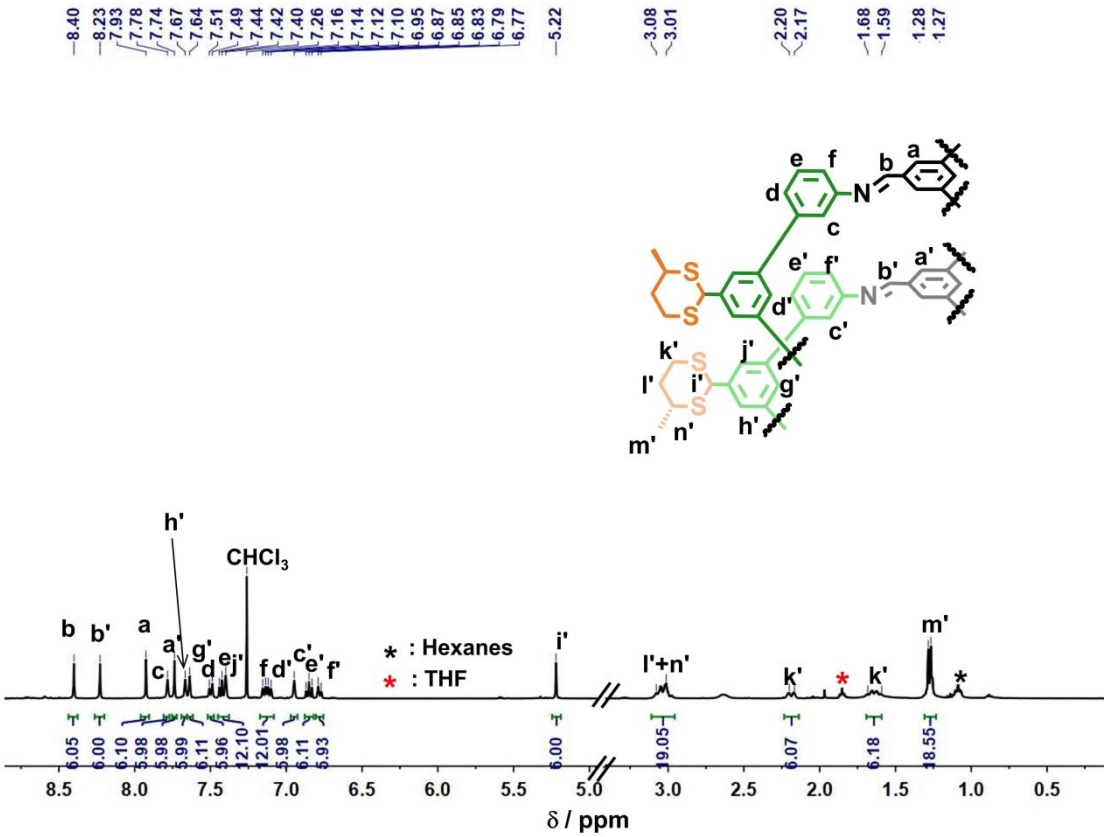

Figure S30. ^{1}H NMR spectrum of enantiopure (***S***, ***R***)^{6}-**3** in $CDCl_3$.

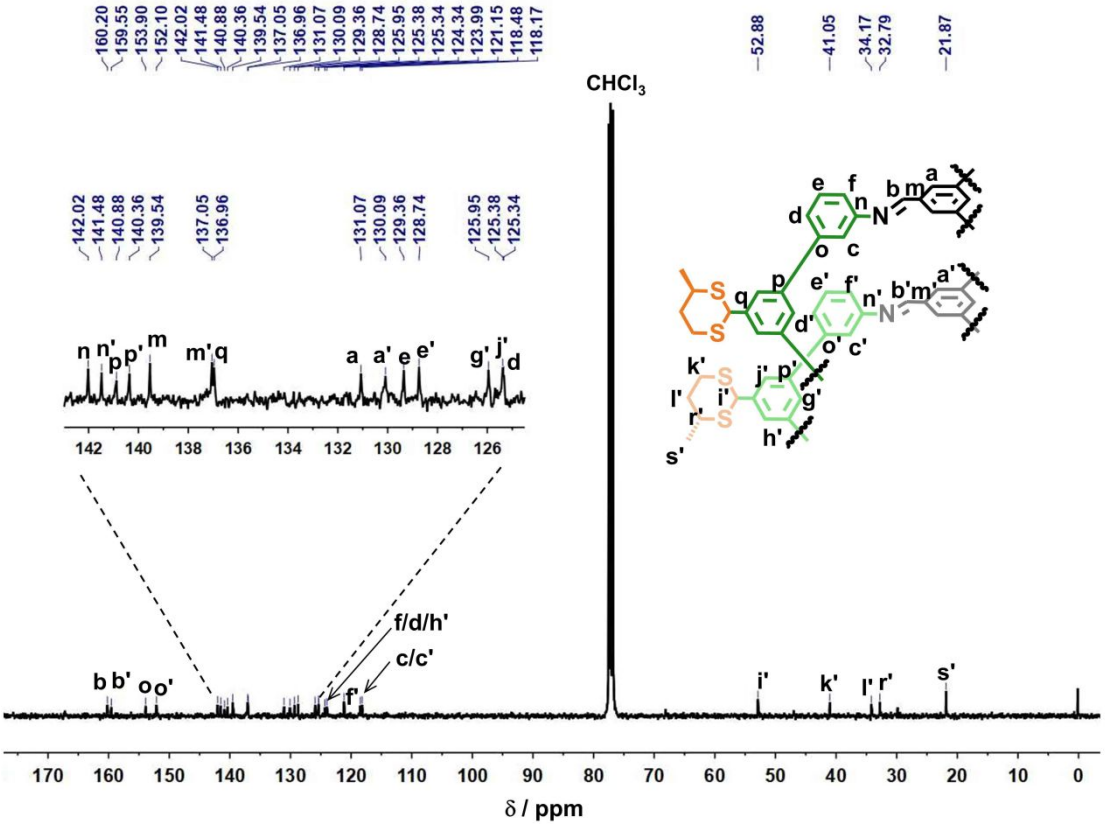

Figure S31. ^{13}C NMR spectrum of enantiopure (***S***, ***R***)^{6}-**3** in $CDCl_3$.

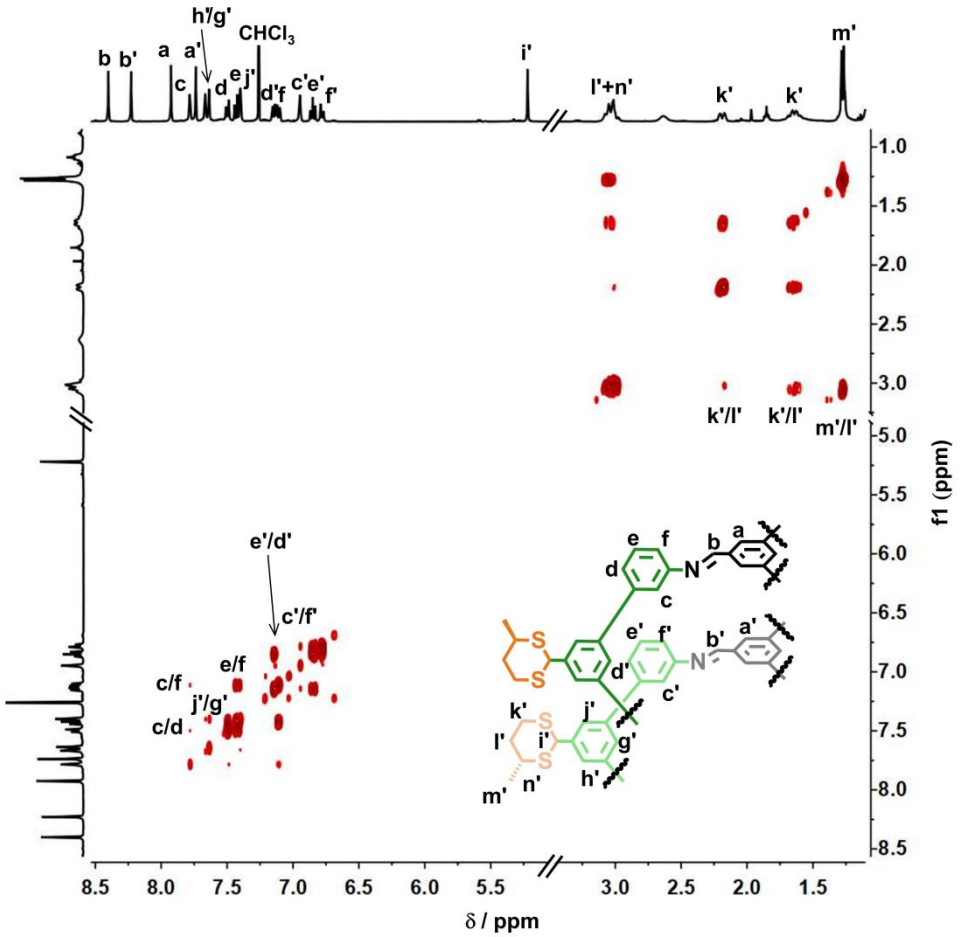

Figure S32. ^{1}H-^{1}H COSY spectrum of enantiopure (***S***, ***R***)^{6}-**3** in $CDCl_3$.

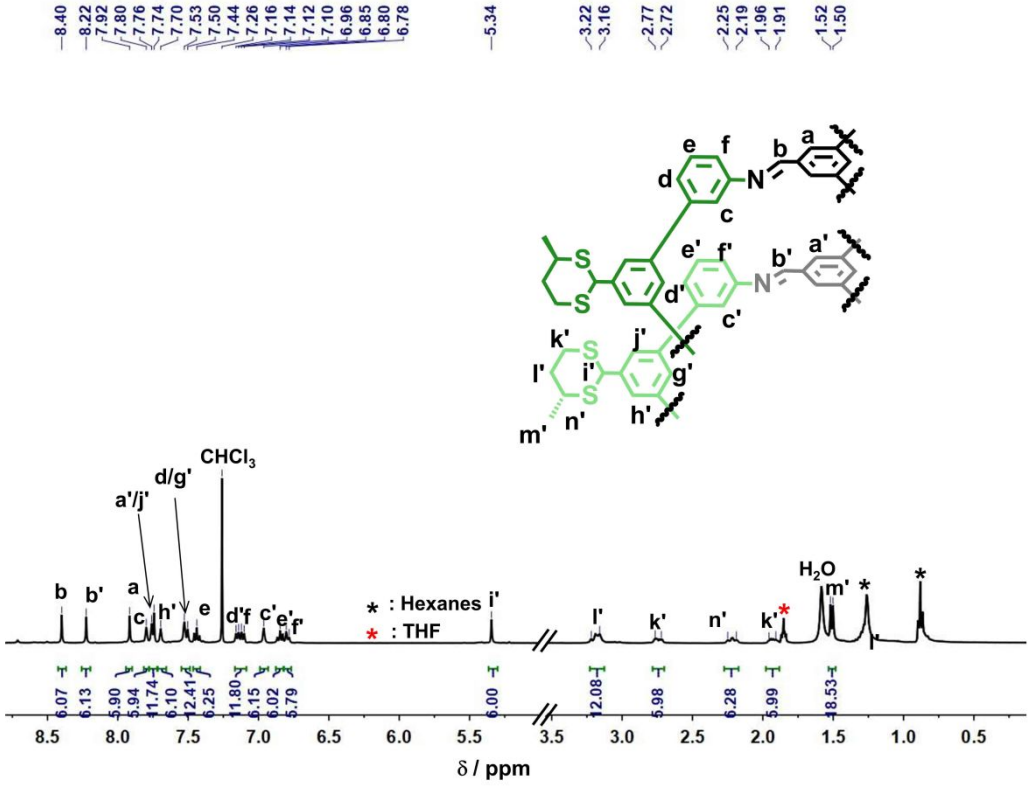

Figure S33. ^{1}H NMR spectrum of enantiopure (***R***, ***R***)^{6}-**3** in $CDCl_3$.

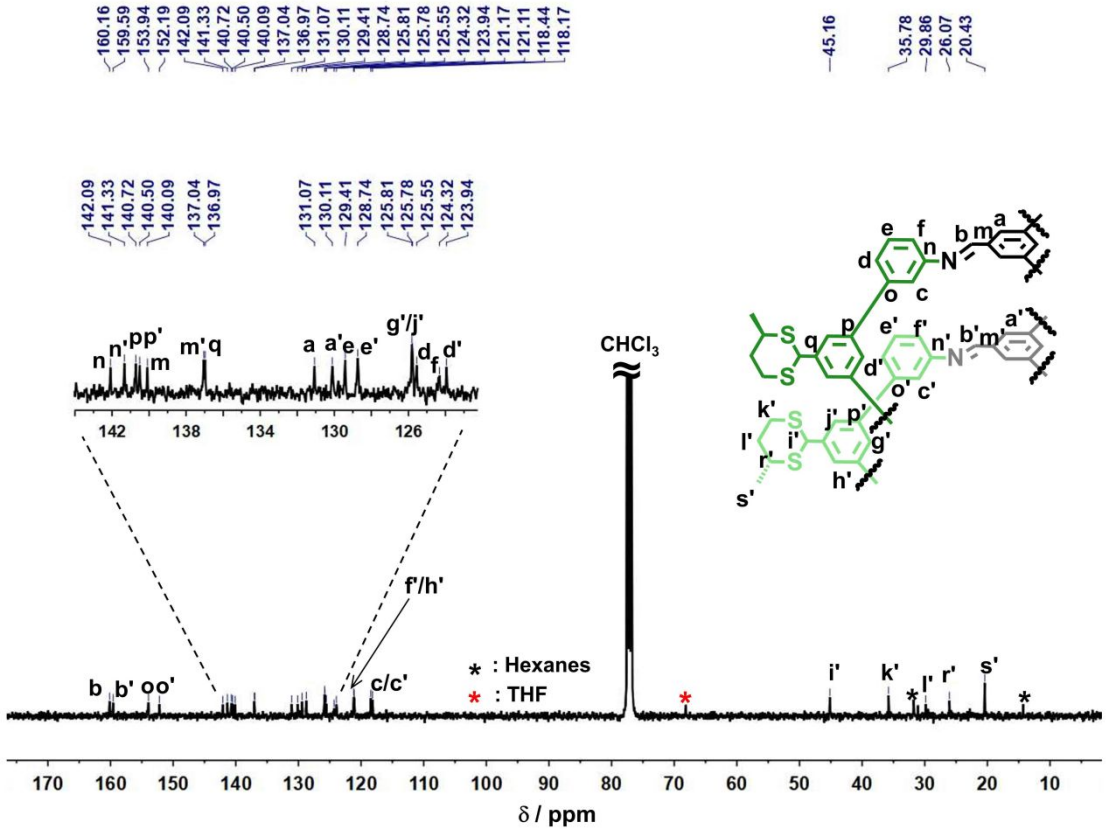

Figure S34. ^{13}C NMR spectrum of enantiopure (***R***, ***R***)^{6}-**3** in $CDCl_3$.

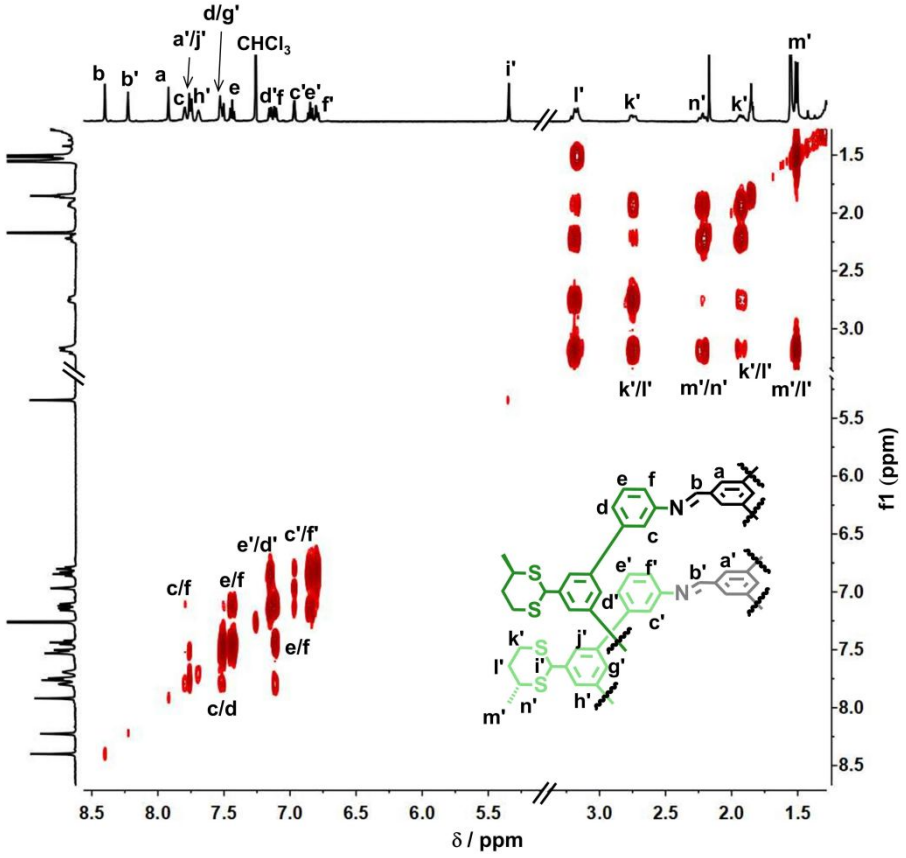

Figure S35. ^{1}H-^{1}H COSY spectrum of enantiopure (***R***, ***R***)^{6}-**3** in $CDCl_3$.

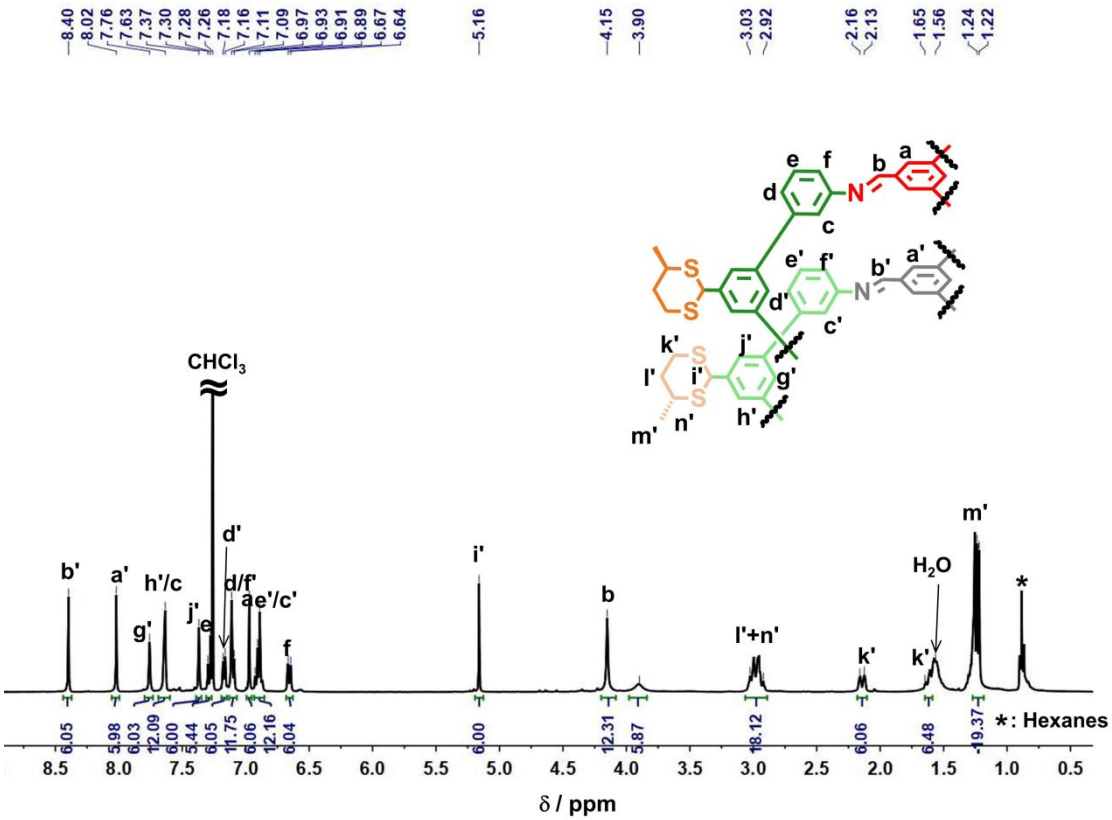

Figure S36. ^{1}H NMR spectrum of enantiopure (***S***, ***R***)^{6}-**4** in $CDCl_3$.

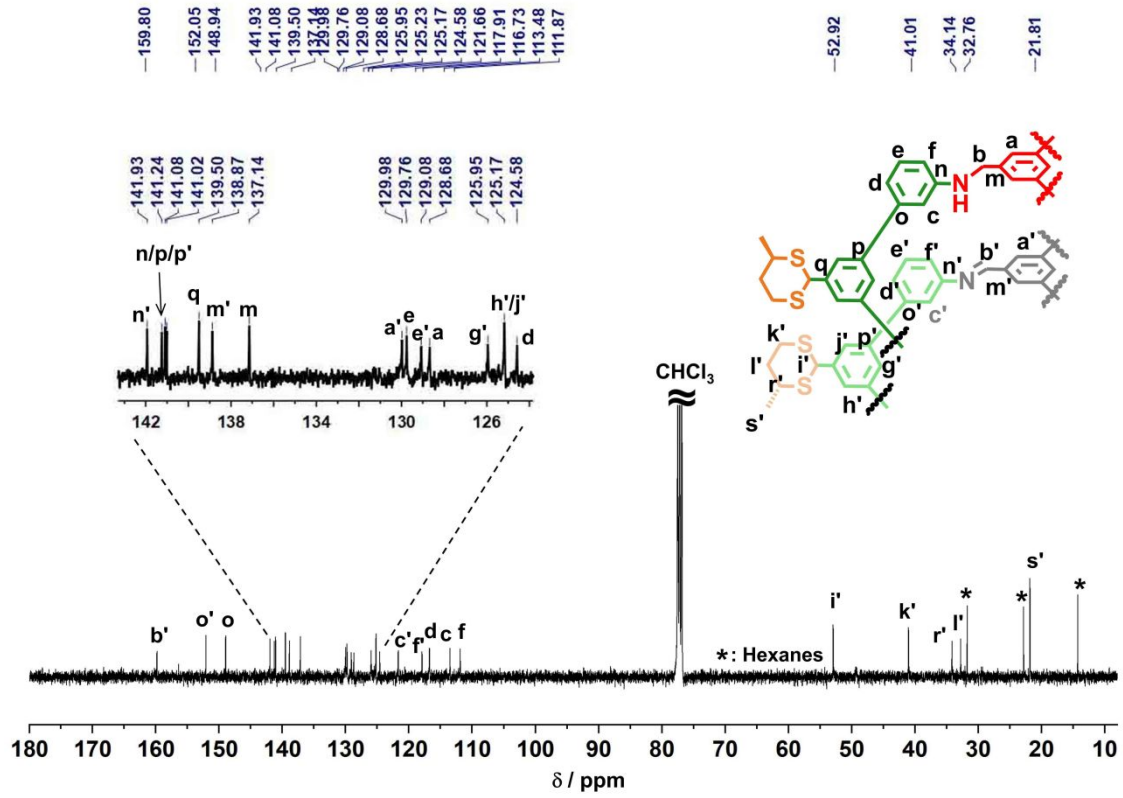

Figure S37. ^{13}C NMR spectrum of enantiopure (***S***, ***R***)^{6}-**4** in $CDCl_3$.

9. MALDI-TOF MS Spectrum of Cage-Catenanes

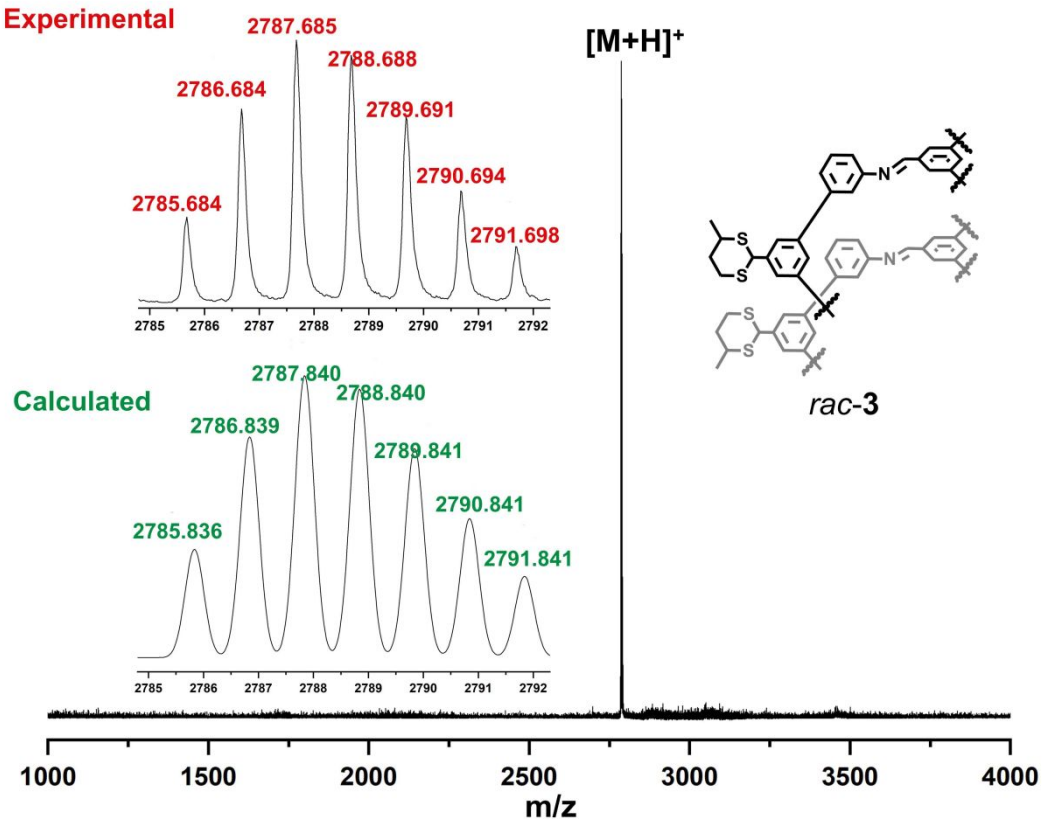

Figure S38. Calculated and experimental MALDI-TOF MS spectra of *rac*-**3**.

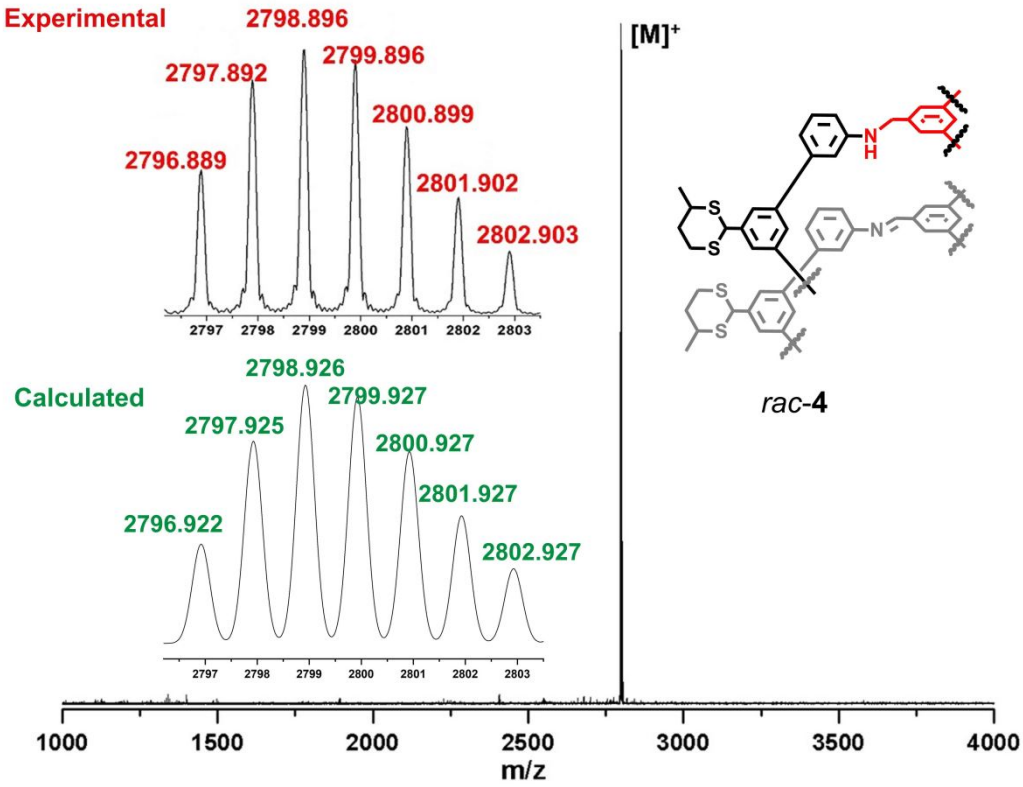

Figure S39. Calculated and experimental MALDI-TOF MS spectra of *rac*-**4**.

10. References

(S1) P. Li, S. Xu, C. Yu, Z.-Y. Li, J. Xu, Z.-M. Li, L. Zou, X. Leng, S. Gao, Liu,Z.; X. Liu, S. Zhang, *Angew. Chem. Int. Ed*. **2020**, *59*, 7113–7121.

(S2) O. V. Dolomanov, L. J. Bourhis, R. J. Gildea, J. A. K. Howard, H. Puschmann, *J. Appl.Cryst.* **2009**, *42*, 339–341.

(S3) G. M. Sheldrick, *Acta Cryst*. **2015**, *A71*, 3–8.

(S4) G. M. Sheldrick, *Acta Cryst*. **2015**, *C71,* 3–8.

(S5) Gaussian 09, revision D. 01, M. J. Frisch, G. W. Trucks, H. B. Schlegel, G. E. Scuseria, M. A. Robb, J. R. Cheeseman, G. Scalmani, V. Barone, B. Mennucci, G. A. Petersson, H. Nakatsuji, M. Caricato, X. Li, H. P. Hratchian, A. F. Izmaylov, J. Bloino, G. Zheng, J. L. Sonnenberg, M. Hada, M. Ehara, K. Toyota, R. Fukuda, J. Hasegawa, M. Ishida, T. Nakajima, Y. Honda, O. Kitao, H. Nakai, T. Vreven, J. Montgomery, J. A. J. E. Peralta, F. Ogliaro, M. Bearpark, J. J. Heyd, E. Brothers, K. N. Kudin, V. N. Staroverov, R. Kobayashi, J. Normand, K. Raghavachari, A. Rendell, J. C. Burant, S. S. Iyengar, J. Tomasi, M. Cossi, N. Rega, N. J. Millam, M. Klene, J. E. Knox, J. B. Cross, V. Bakken, C. Adamo, J. Jaramillo, R. Gomperts, R. E. Stratmann, O. Yazyev, A. J. Austin, R. Cammi, C. Pomelli, J. W. Ochterski, R. L. Martin, K. Morokuma, V. G. Zakrzewski, G. A. Voth, P. Salvador, J. J. Dannenberg, S. Dapprich, A. D. Daniels, O. Farkas, J. B. Foresman, J. V. Ortiz, J. Cioslowski, D. J. Fox, Gaussian, Inc. Wallingford CT, **2013**.

(S6) S. Vosko, L. Wilk, M. Nusair, *Can. J. Phys.* **1980**, *58,* 1200–1211.

(S7) A. D. Becke, *J. Chem. Phys.* **1997**, *107,* 8554–8560.

(S8) W. Kohn, A. D. Becke, R. G. Parr, *J. Phys. Chem.* **1996**, *100,* 12974–12980.